

Velocity-scalar filtered density function for large eddy simulation of turbulent flows

M. R. H. Sheikhi, T. G. Drozda, and P. Givi^{a)}

Department of Mechanical Engineering, University of Pittsburgh, Pittsburgh, Pennsylvania 15261

S. B. Pope

Sibley School of Mechanical and Aerospace Engineering, Cornell University, Ithaca, New York 14853-1301

(Received 7 October 2002; accepted 22 April 2003; published 2 July 2003)

A methodology termed the “velocity-scalar filtered density function” (VSFDF) is developed and implemented for large eddy simulation (LES) of turbulent flows. In this methodology, the effects of the unresolved subgrid scales (SGS) are taken into account by considering the joint probability density function (PDF) of the velocity and scalar fields. An exact transport equation is derived for the VSFDF in which the effects of the SGS convection and chemical reaction are closed. The unclosed terms in this equation are modeled in a fashion similar to that typically used in Reynolds-averaged simulation procedures. A system of stochastic differential equations (SDEs) which yields statistically equivalent results to the modeled VSFDF transport equation is constructed. These SDEs are solved numerically by a Lagrangian Monte Carlo procedure in which the Itô–Gikhman character of the SDEs is preserved. The consistency of the proposed SDEs and the convergence of the Monte Carlo solution are assessed by comparison with results obtained by a finite difference LES procedure in which the corresponding transport equations for the first two SGS moments are solved. The VSFDF results are compared with those obtained by the Smagorinsky model, and all the results are assessed via comparison with data obtained by direct numerical simulation of a temporally developing mixing layer involving transport of a passive scalar. It is shown that the values of both the SGS and the resolved components of all second order moments including the scalar fluxes are predicted well by VSFDF. The sensitivity of the calculations to the model’s (empirical) constants are assessed and it is shown that the magnitudes of these constants are in the same range as those employed in PDF methods. © 2003 American Institute of Physics.

[DOI: 10.1063/1.1584678]

I. INTRODUCTION

The probability density function (PDF) approach has proven useful for large eddy simulation (LES) of turbulent reacting flows.¹ The formal means of conducting such LES is by considering the “filtered density function” (FDF)² which is essentially the filtered fine-grained PDF of the transport quantities. In all previous contributions, the “marginal” FDF of the scalars,^{3–15} or the marginal FDF of the velocity vector¹⁶ are considered; see Givi¹⁷ for a recent review.

The objective of the present work is to extend the FDF methodology to account for the “joint” subgrid scale (SGS) velocity and scalar fields. This is accomplished by considering the joint “velocity-scalar filtered density function” (VSFDF). With the definition of the VSFDF, the mathematical framework for its implementation in LES is established. A transport equation is developed for the VSFDF in which the effects of SGS convection and SGS chemical reaction (in a reacting flow) are closed. The unclosed terms in this equation are modeled in a fashion similar to those in the Reynolds-averaged simulation (RAS) procedures. A La-

grangian Monte Carlo procedure is developed and implemented for numerical simulation of the modeled VSFDF transport equation. The consistency of this procedure is assessed by comparing the first two moments of the VSFDF with those obtained by the Eulerian finite difference solutions of the same moments’ transport equations. The results of the VSFDF simulations are compared with those predicted by the Smagorinsky¹⁸ closure. All the results are assessed via comparisons with direct numerical simulation (DNS) data of a three-dimensional (3D) temporally developing mixing layer involving transport of a passive scalar variable. The sensitivity of VSFDF predictions to the values of the model’s (empirical) constants is assessed.

II. FORMULATION

For the general formulation, we consider an incompressible (unit density), isothermal, turbulent reacting flow involving N_s species. The primary transport variables describing such a flow are the three components of the velocity vector $u_i(\mathbf{x}, t)$ ($i = 1, 2, 3$), the pressure $p(\mathbf{x}, t)$, and the species’ mass fractions $\phi_\alpha(\mathbf{x}, t)$ ($\alpha = 1, 2, \dots, N_s$). The equations which govern the transport of these variables in space (x_i) and time (t) are

^{a)} Author to whom correspondence should be addressed. Telephone: (412) 624-9605; fax: 716-624-4846; electronic mail: givi@engr.pitt.edu

$$\frac{\partial u_k}{\partial x_k} = 0, \quad (1a)$$

$$\frac{\partial u_i}{\partial t} + \frac{\partial u_k u_i}{\partial x_k} = -\frac{\partial p}{\partial x_i} + \frac{\partial \sigma_{ik}}{\partial x_k}, \quad (1b)$$

$$\frac{\partial \phi_\alpha}{\partial t} + \frac{\partial u_k \phi_\alpha}{\partial x_k} = -\frac{\partial J_k^\alpha}{\partial x_k} + S_\alpha, \quad (1c)$$

where $S_\alpha \equiv \hat{S}_\alpha(\boldsymbol{\phi}(\mathbf{x}, t))$ denotes the chemical reaction term for species α , and $\boldsymbol{\phi} = [\phi_1, \phi_2, \dots, \phi_{N_s}]$ denotes the scalar variable array. For an incompressible, Newtonian fluid, with Fick's law of diffusion, the viscous stress tensor σ_{ik} and the scalar flux J_k^α are represented by

$$\sigma_{ik} = \nu \left(\frac{\partial u_i}{\partial x_k} + \frac{\partial u_k}{\partial x_i} \right), \quad (2a)$$

$$J_k^\alpha = -\Gamma \frac{\partial \phi_\alpha}{\partial x_k}, \quad (2b)$$

where ν is the fluid kinematic viscosity and $\Gamma = \nu / \text{Sc}$ is the diffusion coefficient of all species with Sc denoting the molecular Schmidt number. We assume a constant value for $\nu = \Gamma$; i.e., $\text{Sc} = 1$. In reactive flows, molecular processes are much more complicated than portrayed by Eq. (2). Since the molecular diffusion is typically less important than that of SGS, this simple model is adopted with justifications and caveats given in Refs. 19–21.

Large eddy simulation involves the spatial filtering operation^{1,22–25}

$$\langle f(\mathbf{x}, t) \rangle = \int_{-\infty}^{+\infty} f(\mathbf{x}', t) G(\mathbf{x}', \mathbf{x}) d\mathbf{x}', \quad (3)$$

where $G(\mathbf{x}', \mathbf{x})$ denotes a filter function, and $\langle f(\mathbf{x}, t) \rangle$ is the filtered value of the transport variable $f(\mathbf{x}, t)$. We consider a filter function that is spatially and temporally invariant and localized, thus: $G(\mathbf{x}', \mathbf{x}) \equiv G(\mathbf{x}' - \mathbf{x})$ with the properties $G(\mathbf{x}) \geq 0$, $\int_{-\infty}^{+\infty} G(\mathbf{x}) d\mathbf{x} = 1$. Applying the filtering operation to Eqs. (1) yields

$$\frac{\partial \langle u_k \rangle}{\partial x_k} = 0, \quad (4a)$$

$$\frac{\partial \langle u_i \rangle}{\partial t} + \frac{\partial \langle u_k \rangle \langle u_i \rangle}{\partial x_k} = -\frac{\partial \langle p \rangle}{\partial x_i} + \nu \frac{\partial^2 \langle u_i \rangle}{\partial x_k \partial x_k} - \frac{\partial \tau(u_k, u_i)}{\partial x_k}, \quad (4b)$$

$$\frac{\partial \langle \phi_\alpha \rangle}{\partial t} + \frac{\partial \langle u_k \rangle \langle \phi_\alpha \rangle}{\partial x_k} = \nu \frac{\partial^2 \langle \phi_\alpha \rangle}{\partial x_k \partial x_k} - \frac{\partial \tau(u_k, \phi_\alpha)}{\partial x_k} + \langle S_\alpha \rangle, \quad (4c)$$

where the second-order SGS correlations

$$\tau(a, b) = \langle ab \rangle - \langle a \rangle \langle b \rangle \quad (5)$$

are governed by

$$\begin{aligned} & \frac{\partial \tau(u_i, u_j)}{\partial t} + \frac{\partial \langle u_k \rangle \tau(u_i, u_j)}{\partial x_k} \\ &= \nu \frac{\partial^2 \tau(u_i, u_j)}{\partial x_k \partial x_k} - \tau(u_k, u_i) \frac{\partial \langle u_j \rangle}{\partial x_k} - \tau(u_k, u_j) \frac{\partial \langle u_i \rangle}{\partial x_k} \\ & \quad - \left[2\nu \tau \left(\frac{\partial u_i}{\partial x_k}, \frac{\partial u_j}{\partial x_k} \right) + \tau \left(u_i, \frac{\partial p}{\partial x_j} \right) + \tau \left(u_j, \frac{\partial p}{\partial x_i} \right) \right] \\ & \quad - \frac{\partial \tau(u_k, u_i, u_j)}{\partial x_k}, \end{aligned} \quad (6a)$$

$$\begin{aligned} & \frac{\partial \tau(u_i, \phi_\alpha)}{\partial t} + \frac{\partial \langle u_k \rangle \tau(u_i, \phi_\alpha)}{\partial x_k} \\ &= \nu \frac{\partial^2 \tau(u_i, \phi_\alpha)}{\partial x_k \partial x_k} - \tau(u_k, u_i) \frac{\partial \langle \phi_\alpha \rangle}{\partial x_k} - \tau(u_k, \phi_\alpha) \frac{\partial \langle u_i \rangle}{\partial x_k} \\ & \quad - \left[2\nu \tau \left(\frac{\partial u_i}{\partial x_k}, \frac{\partial \phi_\alpha}{\partial x_k} \right) + \tau \left(\phi_\alpha, \frac{\partial p}{\partial x_i} \right) + \tau(u_i, S_\alpha) \right] \\ & \quad - \frac{\partial \tau(u_k, u_i, \phi_\alpha)}{\partial x_k}, \end{aligned} \quad (6b)$$

$$\begin{aligned} & \frac{\partial \tau(\phi_\alpha, \phi_\beta)}{\partial t} + \frac{\partial \langle u_k \rangle \tau(\phi_\alpha, \phi_\beta)}{\partial x_k} \\ &= \nu \frac{\partial^2 \tau(\phi_\alpha, \phi_\beta)}{\partial x_k \partial x_k} - \tau(u_k, \phi_\alpha) \frac{\partial \langle \phi_\beta \rangle}{\partial x_k} \\ & \quad - \tau(u_k, \phi_\beta) \frac{\partial \langle \phi_\alpha \rangle}{\partial x_k} \\ & \quad - \left[2\nu \tau \left(\frac{\partial \phi_\alpha}{\partial x_k}, \frac{\partial \phi_\beta}{\partial x_k} \right) + \tau(\phi_\alpha, S_\beta) + \tau(\phi_\beta, S_\alpha) \right] \\ & \quad - \frac{\partial \tau(u_k, \phi_\alpha, \phi_\beta)}{\partial x_k}. \end{aligned} \quad (6c)$$

In this equation, the third-order correlations

$$\begin{aligned} \tau(a, b, c) &= \langle abc \rangle - \langle a \rangle \tau(b, c) - \langle b \rangle \tau(a, c) \\ & \quad - \langle c \rangle \tau(a, b) - \langle a \rangle \langle b \rangle \langle c \rangle \end{aligned} \quad (7)$$

are unclosed along with the other terms within square brackets.

III. VELOCITY-SCALAR FILTERED DENSITY FUNCTION (VSFDF)

A. Definitions

The “velocity-scalar filtered density function” (VSFDF), denoted by P , is formally defined as²

$$P(\mathbf{v}, \boldsymbol{\psi}, \mathbf{x}, t) = \int_{-\infty}^{+\infty} \varrho(\mathbf{v}, \boldsymbol{\psi}, \mathbf{u}(\mathbf{x}', t), \boldsymbol{\phi}(\mathbf{x}', t)) G(\mathbf{x}' - \mathbf{x}) d\mathbf{x}', \quad (8)$$

$$\begin{aligned} & \varrho(\mathbf{v}, \boldsymbol{\psi}, \mathbf{u}(\mathbf{x}, t), \boldsymbol{\phi}(\mathbf{x}, t)) \\ &= \prod_{i=1}^3 \delta(v_i - u_i(\mathbf{x}, t)) \prod_{\alpha=1}^{N_s} \delta(\psi_\alpha - \phi_\alpha(\mathbf{x}, t)), \end{aligned} \quad (9)$$

where δ denotes the delta function, and $\mathbf{v}, \boldsymbol{\psi}$ are the velocity vector and the scalar array in the sample space. The term ϱ is the ‘‘fine-grained’’ density,^{20,26} hence Eq. (8) defines VSFDF as the spatially filtered value of the fine-grained density. With

the condition of a positive filter kernel,²⁷ P has all of the properties of the PDF.²⁰ For further developments it is useful to define the ‘‘conditional filtered value’’ of the variable $Q(\mathbf{x}, t)$ as

$$\langle Q(\mathbf{x}, t) | \mathbf{u}(\mathbf{x}, t) = \mathbf{v}, \boldsymbol{\phi}(\mathbf{x}, t) = \boldsymbol{\psi} \rangle \equiv \langle Q | \mathbf{v}, \boldsymbol{\psi} \rangle = \frac{\int_{-\infty}^{+\infty} Q(\mathbf{x}', t) \varrho(\mathbf{v}, \boldsymbol{\psi}; \mathbf{u}(\mathbf{x}', t), \boldsymbol{\phi}(\mathbf{x}', t)) G(\mathbf{x}' - \mathbf{x}) d\mathbf{x}'}{P(\mathbf{v}, \boldsymbol{\psi}; \mathbf{x}, t)}. \quad (10)$$

Equation (10) implies the following:

(i) for $Q(\mathbf{x}, t) = c, \langle Q(\mathbf{x}, t) | \mathbf{v}, \boldsymbol{\psi} \rangle = c, \quad (11a)$

(ii) for $Q(\mathbf{x}, t) \equiv \hat{Q}(\mathbf{u}(\mathbf{x}, t), \boldsymbol{\phi}(\mathbf{x}, t)), \langle Q(\mathbf{x}, t) | \mathbf{v}, \boldsymbol{\psi} \rangle = \hat{Q}(\mathbf{v}, \boldsymbol{\psi}). \quad (11b)$

(iii) Integral properties,

$$\langle Q(\mathbf{x}, t) \rangle = \int_{-\infty}^{+\infty} \langle Q(\mathbf{x}, t) | \mathbf{v}, \boldsymbol{\psi} \rangle P(\mathbf{v}, \boldsymbol{\psi}; \mathbf{x}, t) d\mathbf{v} d\boldsymbol{\psi}. \quad (11c)$$

From Eqs. (11) it follows that the filtered value of any function of the velocity and/or scalar variables is obtained by its integration over the velocity and scalar sample spaces

$$\langle Q(\mathbf{x}, t) \rangle = \int_{-\infty}^{+\infty} \hat{Q}(\mathbf{v}, \boldsymbol{\psi}) P(\mathbf{v}, \boldsymbol{\psi}; \mathbf{x}, t) d\mathbf{v} d\boldsymbol{\psi}. \quad (12)$$

B. VSFDF transport equations

To develop the VSFDF transport equation, we consider the time derivative of the fine-grained density function [Eq. (9)],

$$\frac{\partial \varrho}{\partial t} = - \left(\frac{\partial u_k}{\partial t} \frac{\partial \varrho}{\partial v_k} + \frac{\partial \phi_\alpha}{\partial t} \frac{\partial \varrho}{\partial \psi_\alpha} \right). \quad (13)$$

Substituting Eqs. (1b) and (1c), and Eqs. (2a) and (2b) into Eq. (13) we obtain

$$\begin{aligned} \frac{\partial \varrho}{\partial t} + \frac{\partial u_k \varrho}{\partial x_k} &= \left(\frac{\partial p}{\partial x_i} - \nu \frac{\partial^2 u_i}{\partial x_k \partial x_k} \right) \frac{\partial \varrho}{\partial v_i} \\ &\quad - \left(\nu \frac{\partial^2 \phi_\alpha}{\partial x_k \partial x_k} + S_\alpha(\boldsymbol{\phi}) \right) \frac{\partial \varrho}{\partial \psi_\alpha}. \end{aligned} \quad (14)$$

Integration of this according to Eq. (8), while employing Eq. (10) results in

$$\begin{aligned} \frac{\partial P}{\partial t} + \frac{\partial v_k P}{\partial x_k} &= \frac{\partial \langle p \rangle}{\partial x_k} \frac{\partial P}{\partial v_k} - \frac{\partial}{\partial \psi_\alpha} [S_\alpha(\boldsymbol{\psi}) P] \\ &\quad + \frac{\partial}{\partial v_k} \left[\left(\left\langle \frac{\partial p}{\partial x_k} \middle| \mathbf{v}, \boldsymbol{\psi} \right\rangle - \frac{\partial \langle p \rangle}{\partial x_k} \right) P \right] \\ &\quad - \frac{\partial}{\partial v_i} \left(\left\langle \nu \frac{\partial^2 u_i}{\partial x_k \partial x_k} \middle| \mathbf{v}, \boldsymbol{\psi} \right\rangle P \right) \\ &\quad - \frac{\partial}{\partial \psi_\alpha} \left(\left\langle \nu \frac{\partial^2 \phi_\alpha}{\partial x_k \partial x_k} \middle| \mathbf{v}, \boldsymbol{\psi} \right\rangle P \right). \end{aligned} \quad (15)$$

This is an exact transport equation for the VSFDF. It is observed that the effects of convection [second term on left-hand side (LHS)] and chemical reaction [the second term on right-hand side (RHS)] appear in closed forms. The unclosed terms denote convective effects in the velocity-scalar sample space. Alternatively, the VSFDF equation can be expressed as

$$\begin{aligned} \frac{\partial P}{\partial t} + \frac{\partial v_k P}{\partial x_k} &= \nu \frac{\partial^2 P}{\partial x_k \partial x_k} + \frac{\partial \langle p \rangle}{\partial x_k} \frac{\partial P}{\partial v_k} - \frac{\partial}{\partial \psi_\alpha} [S_\alpha(\boldsymbol{\psi}) P] \\ &\quad + \frac{\partial}{\partial v_k} \left[\left(\left\langle \frac{\partial p}{\partial x_k} \middle| \mathbf{v}, \boldsymbol{\psi} \right\rangle - \frac{\partial \langle p \rangle}{\partial x_k} \right) P \right] \\ &\quad - \frac{\partial^2}{\partial v_i \partial v_j} \left[\left\langle \nu \frac{\partial u_i \partial u_j}{\partial x_k \partial x_k} \middle| \mathbf{v}, \boldsymbol{\psi} \right\rangle P \right] \\ &\quad - 2 \frac{\partial^2}{\partial v_i \partial \psi_\alpha} \left[\left\langle \nu \frac{\partial u_i \partial \phi_\alpha}{\partial x_k \partial x_k} \middle| \mathbf{v}, \boldsymbol{\psi} \right\rangle P \right] \\ &\quad - \frac{\partial^2}{\partial \psi_\alpha \partial \psi_\beta} \left[\left\langle \nu \frac{\partial \phi_\alpha \partial \phi_\beta}{\partial x_k \partial x_k} \middle| \mathbf{v}, \boldsymbol{\psi} \right\rangle P \right]. \end{aligned} \quad (16)$$

This is also an exact equation, but the unclosed terms are exhibited by the conditional filtered values of the dissipation fields as shown by the last three terms on the RHS.

C. Modeled VSFDF transport equation

For closure of the VSFDF transport equation, we consider the general diffusion process,²⁸ given by the system of stochastic differential equations (SDEs):

$$\begin{aligned} dX_i^+(t) &= D_i^X(\mathbf{X}^+, \mathbf{U}^+, \boldsymbol{\phi}^+; t) dt \\ &\quad + B_{ij}^X(\mathbf{X}^+, \mathbf{U}^+, \boldsymbol{\phi}^+; t) dW_j^X(t) \\ &\quad + F_{ij}^{XU}(\mathbf{X}^+, \mathbf{U}^+, \boldsymbol{\phi}^+; t) dW_j^U(t) \\ &\quad + F_{ij}^{X\phi}(\mathbf{X}^+, \mathbf{U}^+, \boldsymbol{\phi}^+; t) dW_j^\phi(t), \end{aligned} \quad (17a)$$

$$\begin{aligned} dU_i^+(t) &= D_i^U(\mathbf{X}^+, \mathbf{U}^+, \boldsymbol{\phi}^+; t) dt \\ &\quad + B_{ij}^U(\mathbf{X}^+, \mathbf{U}^+, \boldsymbol{\phi}^+; t) dW_j^U(t) \\ &\quad + F_{ij}^{UX}(\mathbf{X}^+, \mathbf{U}^+, \boldsymbol{\phi}^+; t) dW_j^X(t) \\ &\quad + F_{ij}^{U\phi}(\mathbf{X}^+, \mathbf{U}^+, \boldsymbol{\phi}^+; t) dW_j^\phi(t), \end{aligned} \quad (17b)$$

$$\begin{aligned}
 d\phi_\alpha^+(t) = & D_\alpha^\phi(\mathbf{X}^+, \mathbf{U}^+, \boldsymbol{\phi}^+; t) dt \\
 & + B_{\alpha j}^\phi(\mathbf{X}^+, \mathbf{U}^+, \boldsymbol{\phi}^+; t) dW_j^\phi(t) \\
 & + F_{\alpha j}^{\phi X}(\mathbf{X}^+, \mathbf{U}^+, \boldsymbol{\phi}^+; t) dW_j^X(t) \\
 & + F_{\alpha j}^{\phi U}(\mathbf{X}^+, \mathbf{U}^+, \boldsymbol{\phi}^+; t) dW_j^U(t), \tag{17c}
 \end{aligned}$$

where X_i^+ , U_i^+ , ϕ_α^+ are probabilistic representations of position, velocity vector, and scalar variables, respectively. The D terms denote drift in the composition space, the B terms denote diffusion, the F terms denote diffusion couplings, and the W terms denote the Wiener–Lévy processes.^{29,30} Following Haworth and Pope,³¹ Dreeben and Pope,³² Colucci *et al.*,⁷ and Gicquel *et al.*¹⁶ we consider the generalized Langevin model (GLM) and the linear mean square estimation (LMSE) model²⁶

$$dX_i^+ = U_i^+ dt + \sqrt{\nu_1} dW_i^X, \tag{18a}$$

$$\begin{aligned}
 dU_i^+ = & \left[-\frac{\partial \langle p \rangle}{\partial x_i} + \nu_2 \frac{\partial^2 \langle u_i \rangle}{\partial x_k \partial x_k} + G_{ij}(U_j^+ - \langle u_j \rangle) \right] dt \\
 & + \sqrt{\nu_3} \frac{\partial \langle u_i \rangle}{\partial x_k} dW_k^X + \sqrt{C_0 \epsilon} dW_i^U, \tag{18b}
 \end{aligned}$$

$$\begin{aligned}
 d\phi_\alpha^+ = & \left[\nu_{S_1} \frac{\partial^2 \langle \phi_\alpha \rangle}{\partial x_k \partial x_k} - C_\phi \omega (\phi_\alpha^+ - \langle \phi_\alpha \rangle) + S_\alpha \right] dt \\
 & + \sqrt{\nu_{S_2}} \frac{\partial \langle \phi_\alpha \rangle}{\partial x_k} dW_k^X, \tag{18c}
 \end{aligned}$$

where the variables ν_1, ν_2, \dots are all diffusion coefficients (to be specified), and

$$G_{ij} = -\omega \left(\frac{1}{2} + \frac{3}{4} C_0 \right) \delta_{ij}, \quad \omega = \frac{\epsilon}{k}, \tag{19}$$

$$\epsilon = C_\epsilon \frac{k^{3/2}}{\Delta_L}, \quad k = \frac{1}{2} \tau(u_k, u_k).$$

Here ω is the SGS mixing frequency, ϵ is the SGS dissipation rate, k is the SGS kinetic energy, and Δ_L is the LES filter size. The parameters C_0, C_ϕ , and C_ϵ are model constants and need to be specified. The limit $\nu_1 = \nu_3 = \nu_{S_1} = \nu_{S_2} = 0$ is the standard high Reynolds number GLM–LMSE closure.²⁰

The Fokker–Planck equation³³ for $f(\mathbf{v}, \boldsymbol{\psi}, \mathbf{x}; t)$, the joint PDF of $\mathbf{X}^+, \mathbf{U}^+, \boldsymbol{\phi}^+$, evolving by the diffusion process as given by Eq. (18) is

$$\begin{aligned}
 \frac{\partial f}{\partial t} + \frac{\partial}{\partial x_k} (v_k f) = & \left[\frac{\partial \langle p \rangle}{\partial x_i} - (\nu_2 - \sqrt{\nu_1 \nu_3}) \frac{\partial^2 \langle u_i \rangle}{\partial x_k \partial x_k} \right] \frac{\partial f}{\partial v_i} - \frac{\partial}{\partial v_i} [G_{ij}(v_j - \langle u_j \rangle) f] - [\nu_{S_1} - \sqrt{\nu_1 \nu_{S_2}}] \frac{\partial^2 \langle \phi_\alpha \rangle}{\partial x_k \partial x_k} \frac{\partial f}{\partial \psi_\alpha} \\
 & + \frac{\partial}{\partial \psi_\alpha} [C_\phi \omega (\psi_\alpha - \langle \phi_\alpha \rangle) f] - \frac{\partial}{\partial \psi_\alpha} [S_\alpha(\boldsymbol{\psi}) f] + \frac{\nu_1}{2} \frac{\partial^2 f}{\partial x_k \partial x_k} + \sqrt{\nu_1 \nu_3} \frac{\partial \langle u_j \rangle}{\partial x_i} \frac{\partial^2 f}{\partial x_i \partial v_j} \\
 & + \sqrt{\nu_1 \nu_{S_2}} \frac{\partial \langle \phi_\alpha \rangle}{\partial x_i} \frac{\partial^2 f}{\partial x_i \partial \psi_\alpha} + \frac{\nu_3}{2} \frac{\partial \langle u_i \rangle}{\partial x_k} \frac{\partial \langle u_j \rangle}{\partial x_k} \frac{\partial^2 f}{\partial v_i \partial v_j} + \frac{1}{2} C_0 \epsilon \frac{\partial^2 f}{\partial v_k \partial v_k} + \sqrt{\nu_3 \nu_{S_2}} \frac{\partial \langle u_i \rangle}{\partial x_k} \frac{\partial \langle \phi_\alpha \rangle}{\partial x_k} \frac{\partial^2 f}{\partial v_i \partial \psi_\alpha} \\
 & + \frac{\nu_{S_2}}{2} \frac{\partial \langle \phi_\alpha \rangle}{\partial x_k} \frac{\partial \langle \phi_\beta \rangle}{\partial x_k} \frac{\partial^2 f}{\partial \psi_\alpha \partial \psi_\beta}. \tag{20}
 \end{aligned}$$

The transport equations for the filtered variables are obtained by integration of Eq. (20) according to Eq. (12):

$$\frac{\partial \langle u_k \rangle}{\partial x_k} = 0, \tag{21a}$$

$$\frac{\partial \langle u_i \rangle}{\partial t} + \frac{\partial \langle u_k \rangle \langle u_i \rangle}{\partial x_k} = -\frac{\partial \langle p \rangle}{\partial x_i} + \left(\frac{\nu_1}{2} + \nu_2 - \sqrt{\nu_1 \nu_3} \right) \frac{\partial^2 \langle u_i \rangle}{\partial x_k \partial x_k} - \frac{\partial \tau(u_k, u_i)}{\partial x_k}, \tag{21b}$$

$$\frac{\partial \langle \phi_\alpha \rangle}{\partial t} + \frac{\partial \langle u_k \rangle \langle \phi_\alpha \rangle}{\partial x_k} = \left(\nu_{S_1} - \sqrt{\nu_1 \nu_{S_2}} + \frac{\nu_1}{2} \right) \frac{\partial^2 \langle \phi_\alpha \rangle}{\partial x_k \partial x_k} + \langle S_\alpha(\boldsymbol{\phi}) \rangle - \frac{\partial \tau(u_k, \phi_\alpha)}{\partial x_k}. \tag{21c}$$

The transport equations for the second-order SGS moments are

$$\begin{aligned}
 \frac{\partial \tau(u_i, u_j)}{\partial t} + \frac{\partial \langle u_k \rangle \tau(u_i, u_j)}{\partial x_k} = & \frac{\nu_1}{2} \frac{\partial^2 \tau(u_i, u_j)}{\partial x_k \partial x_k} - \tau(u_k, u_i) \frac{\partial \langle u_j \rangle}{\partial x_k} - \tau(u_k, u_j) \frac{\partial \langle u_i \rangle}{\partial x_k} + (\nu_1 - 2\sqrt{\nu_1 \nu_3} + \nu_3) \frac{\partial \langle u_i \rangle}{\partial x_k} \frac{\partial \langle u_j \rangle}{\partial x_k} \\
 & + [G_{ik} \tau(u_k, u_j) + G_{jk} \tau(u_k, u_i) + C_0 \epsilon \delta_{ij}] - \frac{\partial \tau(u_k, u_i, u_j)}{\partial x_k}, \tag{22a}
 \end{aligned}$$

$$\begin{aligned} \frac{\partial \tau(u_i, \phi_\alpha)}{\partial t} + \frac{\partial \langle u_k \rangle \tau(u_i, \phi_\alpha)}{\partial x_k} &= \frac{\nu_1}{2} \frac{\partial^2 \tau(u_i, \phi_\alpha)}{\partial x_k \partial x_k} - \tau(u_k, u_i) \frac{\partial \langle \phi_\alpha \rangle}{\partial x_k} - \tau(u_k, \phi_\alpha) \frac{\partial \langle u_i \rangle}{\partial x_k} \\ &+ (\nu_1 - \sqrt{\nu_1 \nu_3} - \sqrt{\nu_1 \nu_{S_2}} + \sqrt{\nu_3 \nu_{S_2}}) \frac{\partial \langle u_i \rangle}{\partial x_k} \frac{\partial \langle \phi_\alpha \rangle}{\partial x_k} + [G_{ik} \tau(u_k, \phi_\alpha) - C_\phi \omega \tau(u_i, \phi_\alpha)] \\ &+ \tau(u_i, S_\alpha) - \frac{\partial \tau(u_k, u_i, \phi_\alpha)}{\partial x_k}, \end{aligned} \tag{22b}$$

$$\begin{aligned} \frac{\partial \tau(\phi_\alpha, \phi_\beta)}{\partial t} + \frac{\partial \langle u_k \rangle \tau(\phi_\alpha, \phi_\beta)}{\partial x_k} &= \frac{\nu_1}{2} \frac{\partial^2 \tau(\phi_\alpha, \phi_\beta)}{\partial x_k \partial x_k} - \tau(u_k, \phi_\alpha) \frac{\partial \langle \phi_\beta \rangle}{\partial x_k} - \tau(u_k, \phi_\beta) \frac{\partial \langle \phi_\alpha \rangle}{\partial x_k} \\ &+ (\nu_1 - 2\sqrt{\nu_1 \nu_{S_2}} + \nu_{S_2}) \frac{\partial \langle \phi_\alpha \rangle}{\partial x_k} \frac{\partial \langle \phi_\beta \rangle}{\partial x_k} - [2C_\phi \omega \tau(\phi_\alpha, \phi_\beta)] + \tau(\phi_\alpha, S_\beta) \\ &+ \tau(\phi_\beta, S_\alpha) - \frac{\partial \tau(u_k, \phi_\alpha, \phi_\beta)}{\partial x_k}. \end{aligned} \tag{22c}$$

A term-by-term comparison of the exact moment transport equations [Eqs. (4) and (6)], with the modeled equations [Eqs. (21) and (22)], suggests $\nu_1 = \nu_2 = \nu_3 = \nu_{S_1} = \nu_{S_2} = 2\nu$. However, this violates the realizability of the scalar field. A set of coefficients yielding a realizable stochastic model requires: $\nu_1 = \nu_2 = \nu_3 = 2\nu$ and $\nu_{S_1} = \nu_{S_2} = 0$. That is,

$$dX_i^+ = U_i^+ dt + \sqrt{2\nu} dW_i^X, \tag{23a}$$

$$dU_i^+ = \left[-\frac{\partial \langle p \rangle}{\partial x_i} + 2\nu \frac{\partial^2 \langle u_i \rangle}{\partial x_k \partial x_k} + G_{ij}(U_j^+ - \langle u_j \rangle) \right] dt + \sqrt{2\nu} \frac{\partial \langle u_i \rangle}{\partial x_k} dW_k^X + \sqrt{C_0 \epsilon} dW_i^U, \tag{23b}$$

$$d\phi_\alpha^+ = [-C_\phi \omega (\phi_\alpha^+ - \langle \phi_\alpha \rangle) + S_\alpha] dt. \tag{23c}$$

The Fokker–Planck equation for this system is

$$\begin{aligned} \frac{\partial f}{\partial t} + \frac{\partial}{\partial x_k} (v_k f) &= \frac{\partial \langle p \rangle}{\partial x_i} \frac{\partial f}{\partial v_i} - \frac{\partial}{\partial v_i} [G_{ij}(v_j - \langle u_j \rangle) f] + \frac{\partial}{\partial \psi_\alpha} [C_\phi \omega (\psi_\alpha - \langle \phi_\alpha \rangle) f] - \frac{\partial}{\partial \psi_\alpha} [S_\alpha(\psi) f] + \nu \frac{\partial^2 f}{\partial x_k \partial x_k} \\ &+ 2\nu \frac{\partial \langle u_j \rangle}{\partial x_i} \frac{\partial^2 f}{\partial x_i \partial v_j} + \nu \frac{\partial \langle u_i \rangle}{\partial x_k} \frac{\partial \langle u_j \rangle}{\partial x_k} \frac{\partial^2 f}{\partial v_i \partial v_j} + \frac{1}{2} C_0 \epsilon \frac{\partial^2 f}{\partial v_k \partial v_k} \end{aligned} \tag{24}$$

and the corresponding equations for the moments are

$$\frac{\partial \langle u_k \rangle}{\partial x_k} = 0, \tag{25a}$$

$$\frac{\partial \langle u_i \rangle}{\partial t} + \frac{\partial \langle u_k \rangle \langle u_i \rangle}{\partial x_k} = -\frac{\partial \langle p \rangle}{\partial x_i} + \nu \frac{\partial^2 \langle u_i \rangle}{\partial x_k \partial x_k} - \frac{\partial \tau(u_k, u_i)}{\partial x_k}, \tag{25b}$$

$$\frac{\partial \langle \phi_\alpha \rangle}{\partial t} + \frac{\partial \langle u_k \rangle \langle \phi_\alpha \rangle}{\partial x_k} = \nu \frac{\partial^2 \langle \phi_\alpha \rangle}{\partial x_k \partial x_k} + \langle S_\alpha(\phi) \rangle - \frac{\partial \tau(u_k, \phi_\alpha)}{\partial x_k}, \tag{25c}$$

$$\begin{aligned} \frac{\partial \tau(u_i, u_j)}{\partial t} + \frac{\partial \langle u_k \rangle \tau(u_i, u_j)}{\partial x_k} &= \nu \frac{\partial^2 \tau(u_i, u_j)}{\partial x_k \partial x_k} - \tau(u_k, u_i) \frac{\partial \langle u_j \rangle}{\partial x_k} - \tau(u_k, u_j) \frac{\partial \langle u_i \rangle}{\partial x_k} + [G_{ik} \tau(u_k, u_j) + G_{jk} \tau(u_k, u_i) + C_0 \epsilon \delta_{ij}] \\ &- \frac{\partial \tau(u_k, u_i, u_j)}{\partial x_k}, \end{aligned} \tag{26a}$$

$$\begin{aligned} \frac{\partial \tau(u_i, \phi_\alpha)}{\partial t} + \frac{\partial \langle u_k \rangle \tau(u_i, \phi_\alpha)}{\partial x_k} &= \nu \frac{\partial^2 \tau(u_i, \phi_\alpha)}{\partial x_k \partial x_k} - \tau(u_k, u_i) \frac{\partial \langle \phi_\alpha \rangle}{\partial x_k} - \tau(u_k, \phi_\alpha) \frac{\partial \langle u_i \rangle}{\partial x_k} + [G_{ik} \tau(u_k, \phi_\alpha) - C_\phi \omega \tau(u_i, \phi_\alpha)] \\ &+ \tau(u_i, S_\alpha) - \frac{\partial \tau(u_k, u_i, \phi_\alpha)}{\partial x_k}, \end{aligned} \tag{26b}$$

$$\begin{aligned} \frac{\partial \tau(\phi_\alpha, \phi_\beta)}{\partial t} + \frac{\partial \langle u_k \rangle \tau(\phi_\alpha, \phi_\beta)}{\partial x_k} &= \nu \frac{\partial^2 \tau(\phi_\alpha, \phi_\beta)}{\partial x_k \partial x_k} - \tau(u_k, \phi_\alpha) \frac{\partial \langle \phi_\beta \rangle}{\partial x_k} - \tau(u_k, \phi_\beta) \frac{\partial \langle \phi_\alpha \rangle}{\partial x_k} \\ &+ \left[2\nu \frac{\partial \langle \phi_\alpha \rangle}{\partial x_k} \frac{\partial \langle \phi_\beta \rangle}{\partial x_k} - 2C_\phi \omega \tau(\phi_\alpha, \phi_\beta) \right] + \tau(\phi_\alpha, S_\beta) + \tau(\phi_\beta, S_\alpha) - \frac{\partial \tau(u_k, \phi_\alpha, \phi_\beta)}{\partial x_k} \end{aligned} \quad (26c)$$

which may be compared to Eqs. (4) and (6). Therefore, the stochastic diffusion process described by the SDEs (23) implies the following closure for the VSFDF:

$$\begin{aligned} \frac{\partial}{\partial v_k} \left[\left(\left\langle \frac{\partial p}{\partial x_k} \right| \mathbf{v}, \boldsymbol{\psi} \right) - \frac{\partial \langle p \rangle}{\partial x_k} \right] P &- \nu \frac{\partial^2}{\partial v_i \partial v_j} \left[\left\langle \frac{\partial u_i}{\partial x_k} \frac{\partial u_j}{\partial x_k} \right| \mathbf{v}, \boldsymbol{\psi} \right] P - 2\nu \frac{\partial^2}{\partial v_i \partial \psi_\alpha} \left[\left\langle \frac{\partial u_i}{\partial x_k} \frac{\partial \phi_\alpha}{\partial x_k} \right| \mathbf{v}, \boldsymbol{\psi} \right] P \\ &- \nu \frac{\partial^2}{\partial \psi_\alpha \partial \psi_\beta} \left[\left\langle \frac{\partial \phi_\alpha}{\partial x_k} \frac{\partial \phi_\beta}{\partial x_k} \right| \mathbf{v}, \boldsymbol{\psi} \right] P \\ \approx \nu \frac{\partial \langle u_i \rangle}{\partial x_k} \frac{\partial \langle u_j \rangle}{\partial x_k} \frac{\partial^2 P}{\partial v_i \partial v_j} + \frac{1}{2} C_0 \epsilon \frac{\partial^2 P}{\partial v_k \partial v_k} + 2\nu \frac{\partial \langle u_i \rangle}{\partial x_k} \frac{\partial^2 P}{\partial x_k \partial v_i} - \frac{\partial}{\partial v_i} [G_{ij}(v_j - \langle u_j \rangle) P] &+ \frac{\partial}{\partial \psi_\alpha} [C_\phi \omega (\psi_\alpha - \langle \phi_\alpha \rangle) P] \end{aligned} \quad (27)$$

which yields the closures at the second-order levels:

$$\begin{aligned} - \left[2\nu \tau \left(\frac{\partial u_i}{\partial x_k}, \frac{\partial u_j}{\partial x_k} \right) + \tau \left(u_i, \frac{\partial p}{\partial x_j} \right) + \tau \left(u_j, \frac{\partial p}{\partial x_i} \right) \right] \\ = G_{ik} \tau(u_k, u_j) + G_{jk} \tau(u_k, u_i) + C_0 \epsilon \delta_{ij} \\ = -\omega \left(1 + \frac{3}{2} C_0 \right) [\tau(u_i, u_j) - \frac{2}{3} k \delta_{ij}] - \frac{2}{3} \epsilon \delta_{ij}, \end{aligned} \quad (28a)$$

$$\begin{aligned} - \left[2\nu \tau \left(\frac{\partial u_i}{\partial x_k}, \frac{\partial \phi_\alpha}{\partial x_k} \right) + \tau \left(\phi_\alpha, \frac{\partial p}{\partial x_i} \right) \right] \\ = G_{ik} \tau(u_k, \phi_\alpha) - C_\phi \omega \tau(u_i, \phi_\alpha) \\ = -\omega \left(\frac{1}{2} + \frac{3}{4} C_0 + C_\phi \right) \tau(u_i, \phi_\alpha), \end{aligned} \quad (28b)$$

$$\begin{aligned} - 2\nu \tau \left(\frac{\partial \phi_\alpha}{\partial x_k}, \frac{\partial \phi_\beta}{\partial x_k} \right) \\ = -2C_\phi \omega \tau(\phi_\alpha, \phi_\beta) + 2\nu \frac{\partial \langle \phi_\alpha \rangle}{\partial x_k} \frac{\partial \langle \phi_\beta \rangle}{\partial x_k}. \end{aligned} \quad (28c)$$

IV. NUMERICAL SOLUTION PROCEDURE

Numerical solution of the modeled VSFDF transport equation is obtained by a hybrid finite difference-Monte Carlo procedure. The basis is similar to those in RAS^{34–36} and in previous FDF simulations,^{7,9,16} with some differences which are described here. For simulations, the FDF is represented by an ensemble of N_p statistically identical Monte Carlo (MC) particles. Each particle carries information pertaining to its position, $\mathbf{X}^{(n)}(t)$, velocity, $\mathbf{U}^{(n)}(t)$, and scalar value, $\phi^{(n)}(t)$, $n=1, \dots, N_p$. This information is updated via temporal integration of the SDEs. The simplest way of performing this integration is via Euler–Maruyama approximation.³⁷ For example, for Eq. (17a),

$$\begin{aligned} X_i^n(t_{k+1}) &= X_i^n(t_k) + (D_i^X(t_k))^n \Delta t \\ &+ (B_{ij}^X(t_k))^n (\Delta t)^{1/2} (\zeta_j^X(t_k))^n \\ &+ (F_{ij}^{XU}(t_k))^n (\Delta t)^{1/2} (\zeta_j^U(t_k))^n \\ &+ (F_{ij}^{X\phi}(t_k))^n (\Delta t)^{1/2} (\zeta_j^\phi(t_k))^n, \end{aligned} \quad (29)$$

where $D_i(t_k) = D_i(\mathbf{X}^{(n)}(t_k), \mathbf{U}^{(n)}(t_k), \phi^{(n)}(t_k); t_k), \dots$, and $\zeta(t_k)$'s are independent standardized Gaussian random variables. This scheme preserves the Itô character of the SDEs.³⁸

The computational domain is discretized on equally spaced finite difference grid points. These points are used for two purposes: (1) to identify the regions where the statistical

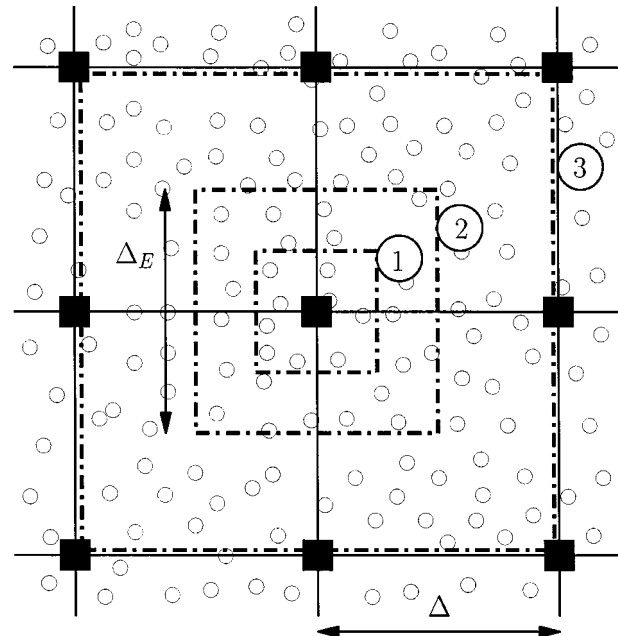


FIG. 1. Concept of ensemble averaging in 2D. Shown are three different ensemble domains: 1 ($\Delta_E = \Delta/2, N_E \approx 10$), 2 ($\Delta_E = \Delta, N_E \approx 40$), 3 ($\Delta_E = 2\Delta, N_E \approx 160$). Solid squares denote the finite-difference grid points, and the circles denote the MC particles.

TABLE I. Attributes of the computational methods.

	LES-FD variables	VSFDF variables	VSFDF quantities used by the LES-FD system	LES-FD quantities used by the VSFDF system	Redundant quantities
VSFDF	$\langle p \rangle, \langle u_i \rangle$ $\langle \phi_\alpha \rangle$	X_i^+ U_i^+ ϕ_α^+	$\tau(u_i, u_j)$ $\tau(u_i, \phi_\alpha)$ $\langle S_\alpha(\phi) \rangle$	$\langle u_i \rangle, \partial \langle p \rangle / \partial x_i$ $\partial \langle u_i \rangle / \partial x_k, \partial^2 \langle u_i \rangle / \partial x_k \partial x_k$ $\langle \phi_\alpha \rangle$	$\langle u_i \rangle$ $\langle \phi_\alpha \rangle$
VSFDF-C	$\langle p \rangle, \langle u_i \rangle$ $\langle \phi_\alpha \rangle$ $\tau(u_i, u_j)$ $\tau(u_i, \phi_\alpha)$ $\tau(\phi_\alpha, \phi_\beta)$	X_i^+ U_i^+ ϕ_α^+	$\tau(u_i, u_j)$ $\tau(u_i, \phi_\alpha)$ $\tau(u_i, u_j, u_k)$ $\tau(u_i, u_j, \phi_\alpha)$ $\tau(u_i, \phi_\alpha, \phi_\beta)$	$\langle u_i \rangle, \partial \langle p \rangle / \partial x_i$ $\partial \langle u_i \rangle / \partial x_k, \partial^2 \langle u_i \rangle / \partial x_k \partial x_k$ $\langle \phi_\alpha \rangle, k$	$\langle u_i \rangle, \langle \phi_\alpha \rangle$ $\tau(u_i, u_j)$ $\tau(u_i, \phi_\alpha)$ $\tau(\phi_\alpha, \phi_\beta)$

information from the MC simulations are obtained; (2) to perform LES primarily by the finite difference methodology which is coupled to the MC solver. The LES procedure via the finite difference discretization is referred to as LES–FD and will be further discussed below.

Statistical information is obtained by considering an ensemble of N_E computational particles residing within an ensemble domain of characteristic length Δ_E centered around each of the finite-difference grid points. This is illustrated schematically in Fig. 1. For reliable statistics with minimal numerical dispersion, it is desired to minimize the size of ensemble domain and maximize the number of the MC particles.²⁰ In this way, the ensemble statistics would tend to the desired filtered values,

$$\begin{aligned}
 \langle a \rangle_E &\equiv \frac{1}{N_E} \sum_{n \in \Delta_E} a^{(n)} \xrightarrow[N_E \rightarrow \infty, \Delta_E \rightarrow 0]{} \langle a \rangle, \\
 \tau_E(a, b) &\equiv \frac{1}{N_E} \sum_{n \in \Delta_E} (a^{(n)} - \langle a \rangle_E)(b^{(n)} - \langle b \rangle_E) \\
 &\xrightarrow[N_E \rightarrow \infty, \Delta_E \rightarrow 0]{} \tau(a, b),
 \end{aligned}
 \tag{30}$$

where $a^{(n)}$ denotes the information carried by n th MC particle pertaining to transport variable a .

The LES–FD solver is based on the compact parameter finite difference scheme.^{39,40} This is a variant of the MacCormack scheme in which fourth-order compact differencing schemes are used to approximate the spatial derivatives, and second-order symmetric predictor–corrector sequence is employed for time discretization. All of the finite difference operations are conducted on fixed grid points. The transfer of information from the grid points to the MC particles is accomplished via a second-order interpolation. The transfer of information from the particles to the grid points is accomplished via ensemble averaging as described above.

The LES–FD procedure determines the pressure field which is used in the MC solver. The LES–FD also determines the filtered velocity and scalar fields. That is, there is a “redundancy” in the determination of the first filtered moments as both the LES–FD and the MC procedures provide the solution of this field. This redundancy is actually very useful in monitoring the accuracy of the simulated results as

shown in previous work.^{9,16,34–36} To establish consistency and convergence of the MC solver, the modeled transport equations for the generalized second-order SGS moments [Eq. (26)] are also solved via LES–FD. In doing so, the unclosed third-order correlations are taken from the MC solver. The comparison of the first and second-order moments as obtained by LES–FD with those obtained by the MC solver is useful to establish the accuracy of the MC solver. These simulations are referred to as VSFDF–C. Attributes of all the simulation procedures are summarized in Table I. In this table and hereinafter, VSFDF simulations refer to the hybrid MC/LES–FD procedure in which the LES–FD is used for only the first-order filtered variables. In VSFDF–C, the LES–FD procedure is used for both first- and second-order filtered values. Further discussions about the simulation methods are available in Refs. 7, 16, 34–36.

V. RESULTS

A. Flows simulated

Simulations are conducted of a two-dimensional (2D) and a 3D incompressible, temporally developing mixing layers involving transport of a passive scalar variable. Since the performance of the model in capturing the velocity-scalar correlations is of primary interest, only nonreacting flow simulations are conducted. Inclusion of chemical reaction via the joint FDF formulation is straightforward and is similar to that in the marginal scalar FDF method.^{7,9–12} The 2D simulations are performed to establish and demonstrate the consistency of the MC solver. The 3D simulations are used to assess the overall predictive capabilities of the VSFDF methodology. These predictions are compared with data obtained by direct numerical simulation (DNS) of the same layer.

The temporal mixing layer consists of two parallel streams travelling in opposite directions with the same speed.^{41–43} In the representation below, x, y (and z) denote the streamwise, the cross-stream (and the spanwise) directions (in 3D), respectively. The velocity components along these directions are denoted by u, v (and w) in the x, y (and z) directions, respectively. Both the filtered streamwise velocity and the scalar fields are initialized with a hyperbolic tangent profiles with $\langle u \rangle = 1, \langle \phi \rangle = 1$ on the top stream and $\langle u \rangle = -1, \langle \phi \rangle = 0$ on the bottom stream. The length L is specified such that $L = 2^N \lambda_u$, where N_p is the desired num-

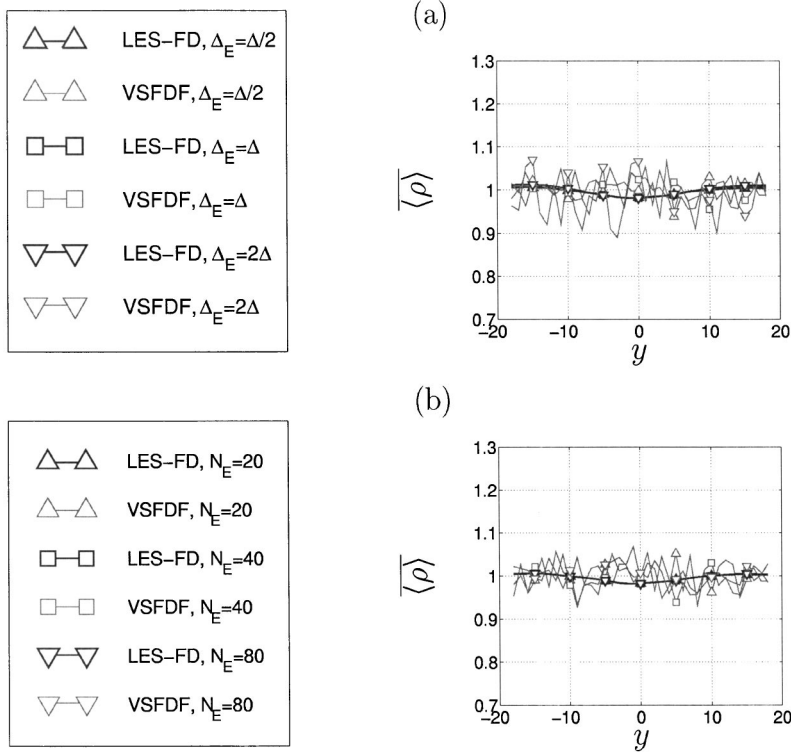


FIG. 2. Cross-stream variation of the Reynolds-averaged values of $\langle \rho \rangle$ at $t = 34.3$: (a) $N_E = 40$, (b) $\Delta_E = \Delta/2$.

ber of successive vortex pairings and λ_u is the wavelength of the most unstable mode corresponding to the mean streamwise velocity profile imposed at the initial time. The flow variables are normalized with respect to the half initial vorticity thickness, $L_r = [\delta_v(t=0)/2]$ ($\delta_v = \Delta U / |\partial \langle u \rangle_L / \partial y|_{\max}$, where $\langle u \rangle_L$ is the Reynolds averaged value of the filtered streamwise velocity and ΔU is the velocity difference across the layer). The reference velocity is $U_r = \Delta U/2$.

All 2D simulations are conducted for $0 \leq x \leq L$, and $-2L/3 \leq y \leq 2L/3$. The formation of large scale structures is facilitated by introducing small harmonic, phase-shifted, disturbances containing subharmonics of the most unstable mode into the streamwise and cross-stream velocity profiles. For $N_p = 1$, this results in formation of two large vortices and one subsequent pairing of these vortices. The 3D simulations are conducted for a cubic box, $0 \leq x \leq L$, $-L/2 \leq y \leq L/2$ ($0 \leq z \leq L$). The 3D field is parametrized in a procedure somewhat similar to that by Vreman *et al.*⁴⁴ The formation of the large scale structures are expedited through eigenfunction based initial perturbations.^{45,46} This includes two-dimensional^{42,44,47} and three-dimensional^{42,48} perturbations with a random phase shift between the 3D modes. This results in the formation of two successive vortex pairings and strong three dimensionality.

B. Numerical specifications

Simulations are conducted on equally spaced grid points with grid spacings $\Delta x = \Delta y = \Delta z$ (for 3D) = Δ . All 2D simulations are performed on 32×41 grid points. The 3D simulations are conducted on 193^3 and 33^3 points for DNS and

LES, respectively. The Reynolds number is $Re = U_r L_r / \nu = 50$. To filter the DNS data, a top-hat function of the form below is used

$$G(\mathbf{x}' - \mathbf{x}) = \prod_{i=1}^3 \tilde{G}(x'_i - x_i), \quad (31)$$

$$\tilde{G}(x'_i - x_i) = \begin{cases} \frac{1}{\Delta_L}, & |x'_i - x_i| \leq \frac{\Delta_L}{2}, \\ 0, & |x'_i - x_i| > \frac{\Delta_L}{2}. \end{cases}$$

No attempt is made to investigate the sensitivity of the results to the filter function²⁷ or the size of the filter.⁴⁹

The MC particles are initially distributed throughout the computational region. All simulations are performed with a uniform “weight”²⁰ of the particles. Due to flow periodicity in the streamwise (and spanwise in 3D) direction(s), if the particle leaves the domain at one of these boundaries new particles are introduced at the other boundary with the same velocity and compositional values. In the cross-stream directions, the free-slip boundary condition is satisfied by the mirror-reflection of the particles leaving through these boundaries. The density of the MC particles is determined by the average number of particles N_E within the ensemble domain of size $\Delta_E \times \Delta_E (\times \Delta_E)$. The effects of both of these parameters are assessed to ensure the consistency and the statistical accuracy of the VSFDF simulations. All results are analyzed both “instantaneously” and “statistically.” In the former, the instantaneous contours (snap-shots) and scatter plots of the variables of interest are analyzed. In the latter,

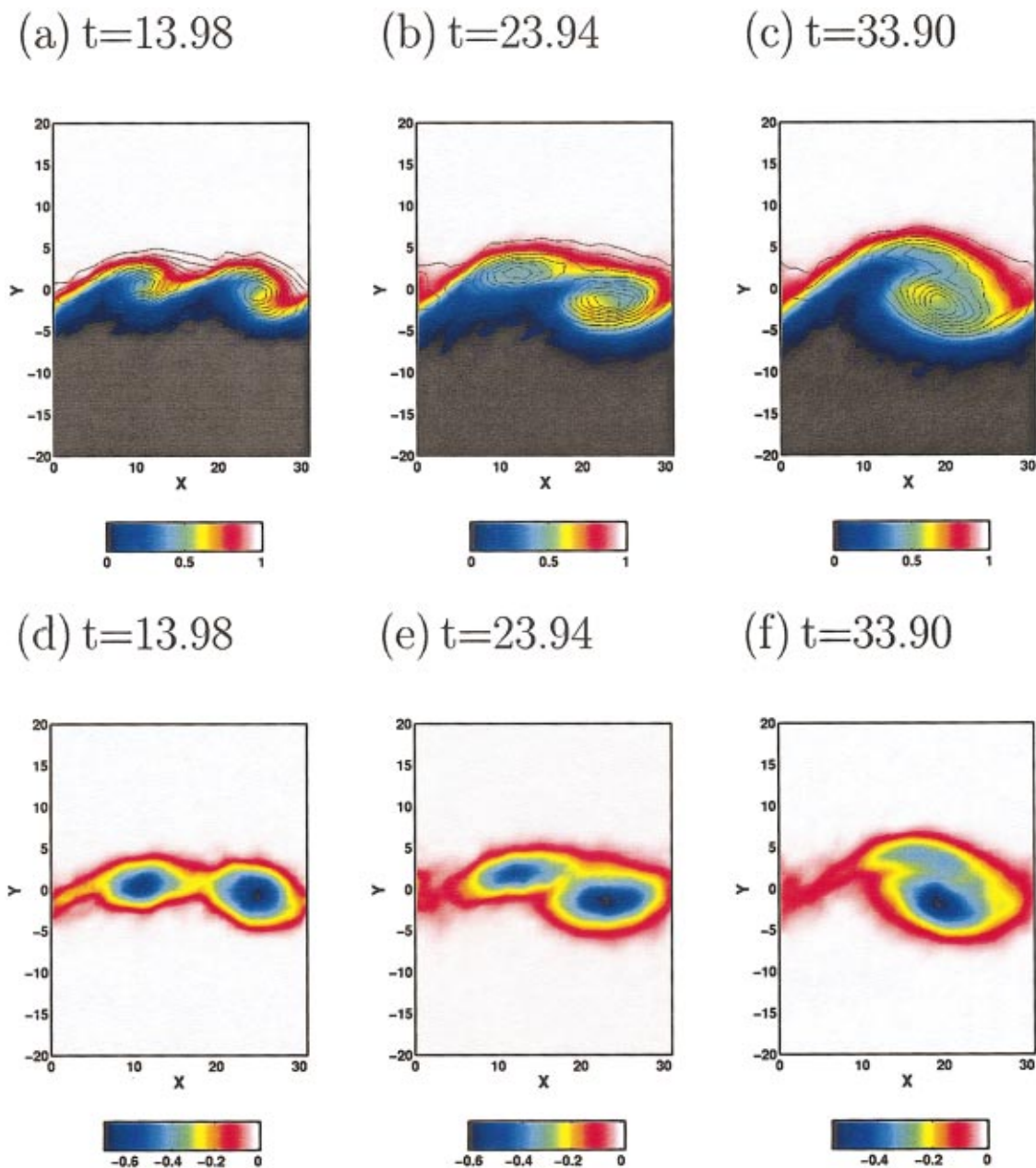


FIG. 3. (Color) Temporal evolution of the scalar (with superimposed vorticity iso-lines) (top) and the vorticity (bottom) fields for LES–FD, with $\Delta_E = \Delta/2$ and $N_E = 40$ at several times.

the “Reynolds-averaged” statistics constructed from the instantaneous data are considered. These are constructed by spatial averaging over x (and z in 3D). All Reynolds-averaged results are denoted by an overbar.

C. Consistency and convergence assessments

The objective of this section is to demonstrate the consistency of the VSFDF formulation and the convergence of its MC simulation procedure. For this purpose, the results via MC and LES–FD are compared against each other in VSFDF–C simulations. Since the accuracy of the FD procedure is well-established (at least for the first-order filtered quantities), such a comparative assessment provides a good means of assessing the performance of the MC solution. No

attempt is made to determine the appropriate values of the model constants; the values suggested in the literature are adopted⁵⁰ $C_0 = 2.1$, $C_\varepsilon = 1$, and $C_\phi = 1$. The influence of these parameters is assessed in Sec. VD.

The uniformity of the MC particles is checked by monitoring their distributions at all times, as the particle number density must be proportional to fluid density. The Reynolds averaged density fields as obtained by both LES–FD and by MC are shown in Fig. 2. Close to unity values for the density at all times is the first measure of the accuracy of simulations. Figures 3 and 4 show the instantaneous contour plots of the filtered scalar and vorticity fields at several times. These figures provide a visual demonstration of the consistency of the VSFDF. This consistency is observed for all first

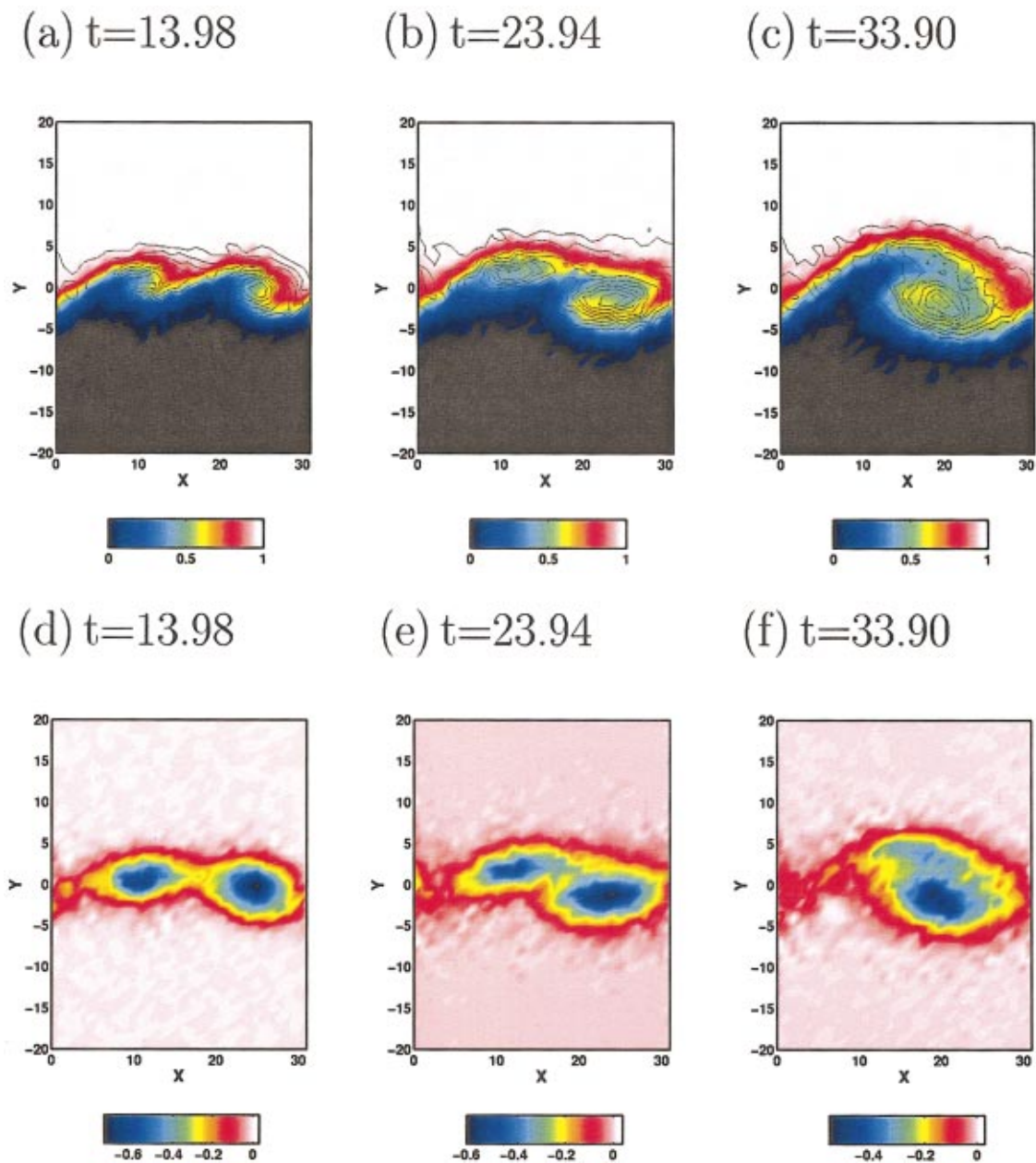


FIG. 4. (Color) Temporal evolution of the scalar (with superimposed vorticity iso-lines) (top) and the vorticity (bottom) fields for VSFDF with $\Delta_E = \Delta/2$ and $N_E = 40$ at several times.

order moments without any statistical variability. Also, all of these moments show very little dependence on the values of Δ_E and N_E consistent with previous FDF simulations.^{7,9,16} In the presentation below we only focus on second-order moments. Specifically, the scalar-velocity correlations are shown since all other second-order SGS moments behave similarly.

Figures 5 and 6 show the statistical variability of the results for simulations with $N_E = 40$. It is observed that these moments exhibit spreads with variances decreasing as the size of the ensemble domain is reduced. Figures 7–10 show the sensitivity to N_E and Δ_E . All these results clearly display convergence suggested by Eq. (30). As the ensemble domain size decreases, the VSFDF results converge to those of LES–

FD. Ideally, the LES–FD results should become independent of the MC results, as the latter become more reliable, i.e., when ($N_E \rightarrow \infty$, $\Delta_E \rightarrow 0$). It is observed that best match is achieved with $\Delta_E \leq \Delta/2$ and $N_E \geq 40$. This conclusion is consistent with previous assessment studies on the scalar FDF,^{7,9} and the velocity FDF.¹⁶ All the subsequent simulations are conducted with $\Delta_E = \Delta/2$ and $N_E = 40$.

D. Comparative assessments of the VSFDF

The objective of this section is to analyze some of the characteristics of the VSFDF via comparative assessments against DNS data. In addition, comparisons are also made with LES via the “conventional” Smagorinsky^{18,51} model:

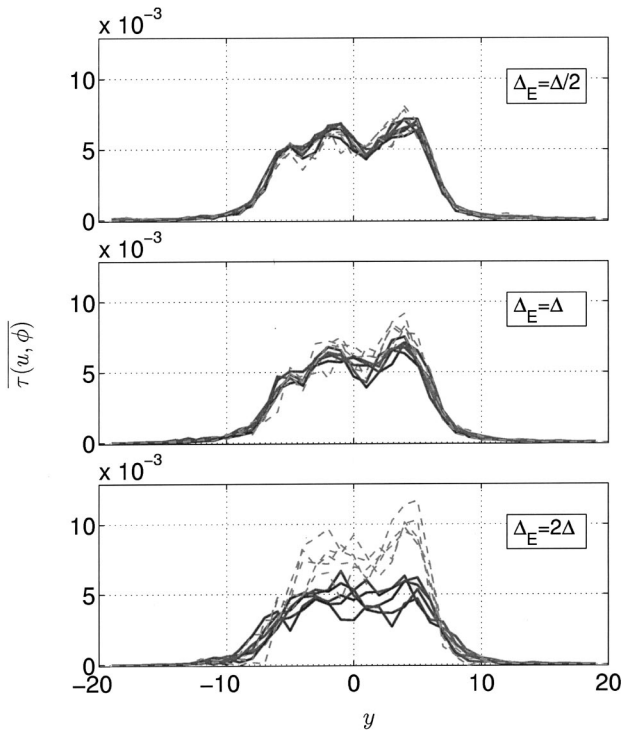


FIG. 5. Statistical variability of LES-FD and VSFDF-C simulations with $N_E=40$ for Reynolds-averaged values of $\tau(u, \phi)$ at $t=34.4$. Solid lines, LES-FD; dashed lines, VSFDF-C.

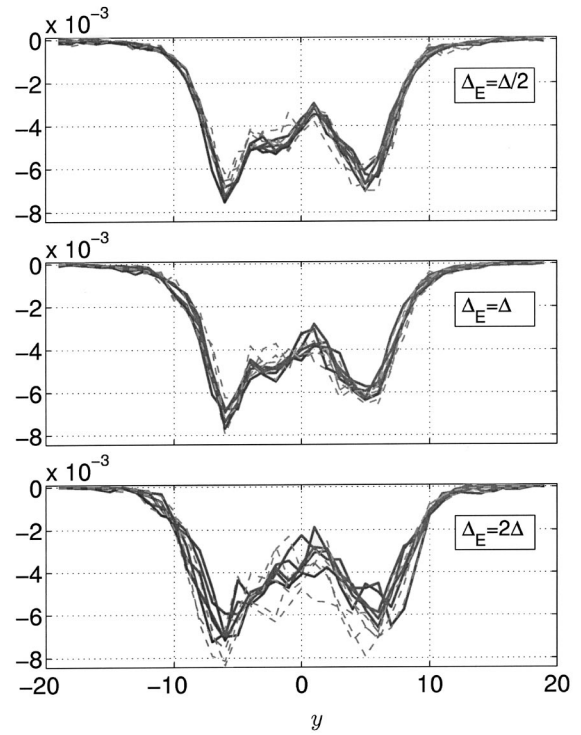


FIG. 6. Statistical variability of LES-FD and VSFDF-C simulations with $N_E=40$ for Reynolds-averaged values of $\tau(v, \phi)$ at $t=34.4$. Solid lines, LES-FD; dashed lines, VSFDF-C.

$$\begin{aligned} \tau_L(u_i, u_j) - \frac{2}{3} k \delta_{ij} &= -2 \nu_t S_{ij}, \\ \tau_L(u_i, \phi) &= -\Gamma_t \frac{\partial \langle \phi \rangle_L}{\partial x_i}, \\ S_{ij} &= \frac{1}{2} \left(\frac{\partial \langle u_i \rangle_L}{\partial x_j} + \frac{\partial \langle u_j \rangle_L}{\partial x_i} \right), \\ \nu_t &= C_\nu \Delta_L^2 S, \quad \Gamma_t = \frac{\nu_t}{Sc_t}. \end{aligned} \tag{32}$$

$C_\nu=0.04$, $Sc_t=1$, $S = \sqrt{S_{ij}S_{ij}}$ and Δ_L is the characteristic length of the filter. This model considers the anisotropic part of the SGS stress tensor $a_{ij} = \tau_L(u_i, u_j) - 2/3k \delta_{ij}$. The isotropic components are absorbed in the pressure field.

For comparison, the DNS data are transposed from the original high resolution 193^3 points to the coarse 33^3 points. In the comparisons, we also consider the “resolved” and the “total” components of the Reynolds-averaged moments. The

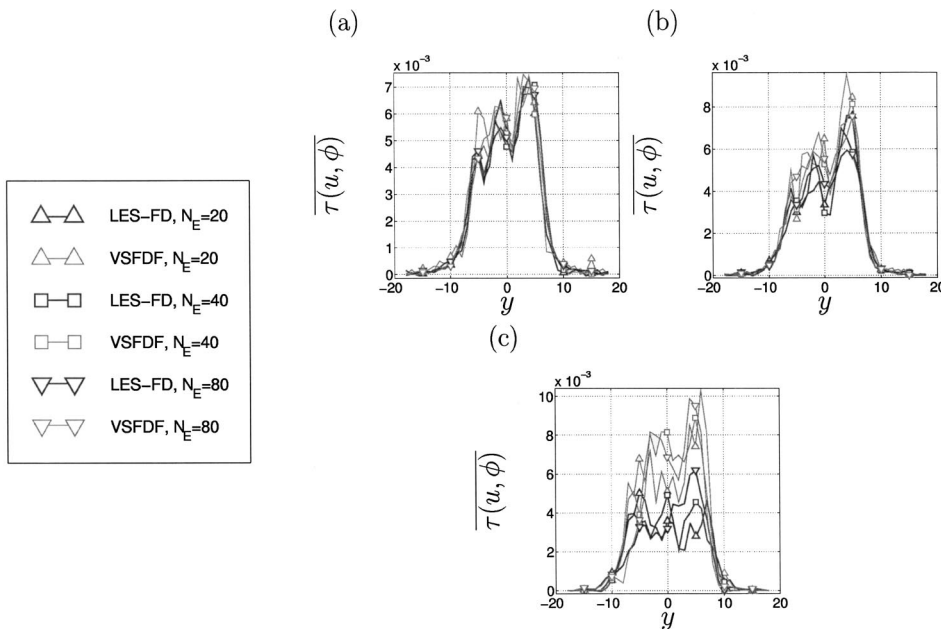


FIG. 7. Cross-stream variations of the Reynolds-averaged values of $\tau(u, \phi)$ (a) $\Delta_E = \Delta/2$, (b) $\Delta_E = \Delta$, (c) $\Delta_E = 2\Delta$.

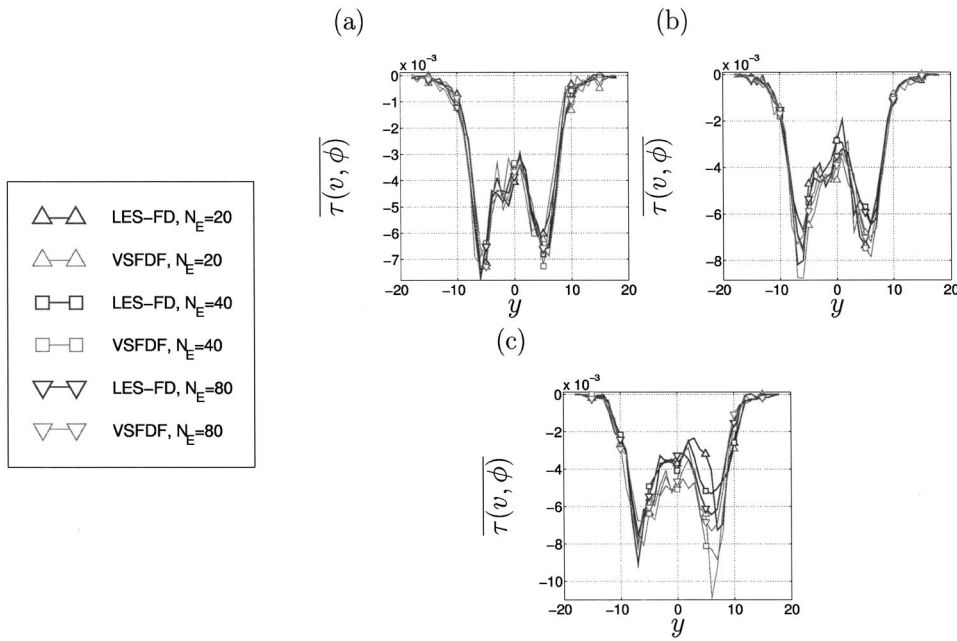


FIG. 8. Cross-stream variations of the Reynolds-averaged values of $\tau(v, \phi)$ (a) $\Delta_E = \Delta/2$, (b) $\Delta_E = \Delta$, (c) $\Delta_E = 2\Delta$.

former are denoted by $\overline{R(a,b)}$ with $R(a,b) = (\langle a \rangle - \langle a \rangle) \times (\langle b \rangle - \langle b \rangle)$; and the latter is $r(a,b)$ with $r(a,b) = (a - \bar{a})(b - \bar{b})$. In DNS, the “total” SGS components are directly available, while in LES they are approximated by $r(a,b) \approx R(a,b) + \tau(a,b)$.⁴⁴ Unless indicated otherwise, the values of the model constants are $C_0 = 2.1$, $C_\epsilon = 1$, $C_\phi = 1$; but the effects of these parameters on the predicted results are assessed.

Figure 11 shows the instantaneous iso-surface of the $\langle \phi \rangle$ field $t = 80$. By this time, the flow has gone through pairings and exhibits strong 3D effects. This is evident by the formation of large scale spanwise rollers with presence of mushroom like structures in streamwise planes.⁴⁵ Similar to previous results,¹⁶ the amount of SGS diffusion with the

Smagorinsky model is significant. Thus, the predicted results are overly smooth. The Reynolds-averaged values of the filtered scalar field at $t = 80$ are shown in Fig. 12, and the temporal variation of the “scalar thickness,”

$$\delta_s(t) = |y(\langle \phi \rangle = 0.9)| + |y(\langle \phi \rangle = 0.1)| \quad (33)$$

is shown in Fig. 13. The filtered and unfiltered DNS data yield virtually indistinguishable results. The dissipative nature of the Smagorinsky model at initial times resulting in a slow growth of the layer is shown. All VSFDF predictions compare well with DNS data in predicting the spread of the layer.

Several components of the planar averaged values of the second-order SGS moments are compared with DNS data in

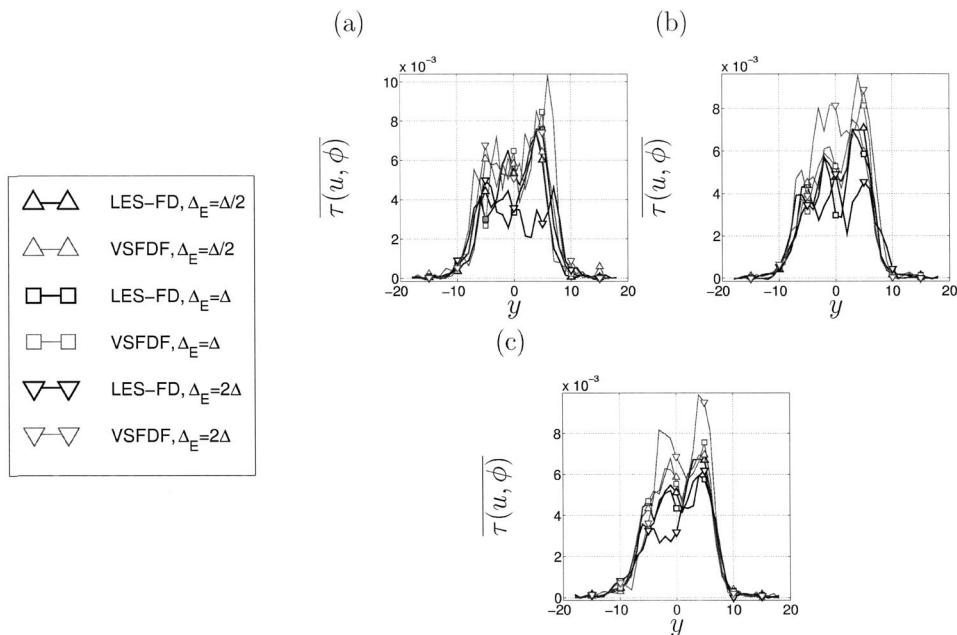


FIG. 9. Cross-stream variations of the Reynolds-averaged values of $\tau(u, \phi)$ (a) $N_E = 20$, (b) $N_E = 40$, (c) $N_E = 80$.

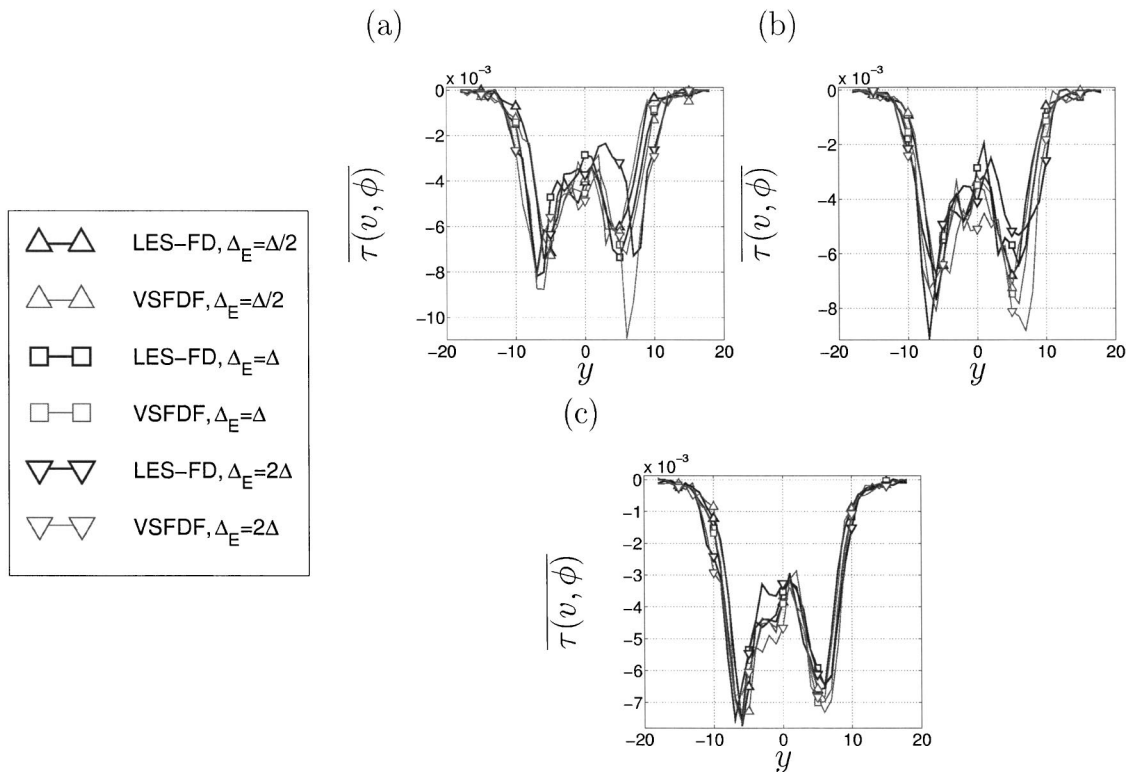


FIG. 10. Cross-stream variations of the Reynolds-averaged values of $\tau(v, \phi)$ (a) $N_E = 20$, (b) $N_E = 40$, (c) $N_E = 80$.

Figs. 14 and 15 for several values of the model constants. In general, the VSFDF results are in better agreement with DNS data than those predicted by the Smagorinsky model. In this regard, therefore, the VSFDF is expected to be more effective than the Smagorinsky type closures for LES of reacting flows since the extent of SGS mixing is heavily influenced by these SGS moments.^{52,53} However, it is not possible to suggest “optimum” values for the model constants, except that at small C_ϵ and C_ϕ values, the SGS energy is very large.

Several components of the resolved second-order moments are presented in Figs. 16 and 17. As expected, the

performance of the Smagorinsky model is not very good as it does not predict the spread and the peak value accurately. The VSFDF yields reasonable predictions except for small C_ϵ values. However, the total values of these moments are fairly independent of the model constants and yield very good agreement with DNS data as shown in Figs. 18 and 19. It is also noted that while the SGS moments and/or the resolved moments may be overestimated and/or underestimated depending on the values of the model coefficients, the total values of the moments are fairly independent of these coefficients, at least in the range of values as considered. But

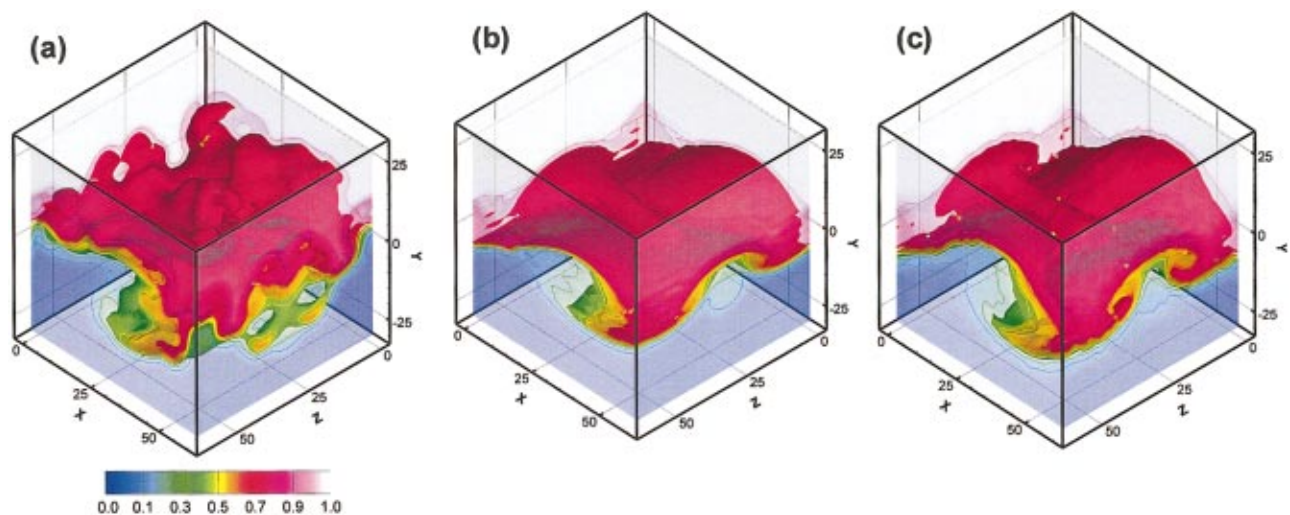


FIG. 11. (Color) Contours surface of the $\langle \phi \rangle$ field in the 3D mixing layer at $t = 80$ as obtained by (a) DNS, (b) Smagorinsky, (c) VSFDF.

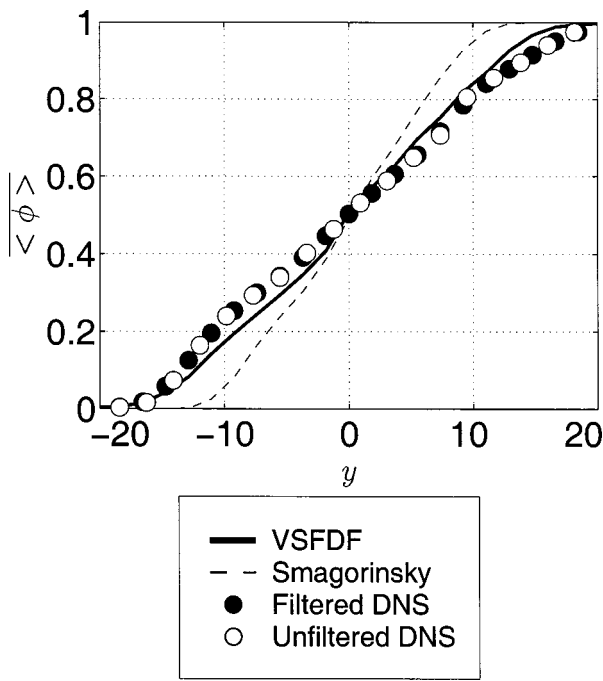


FIG. 12. Cross-stream variations of the Reynolds-averaged values of the filtered scalar field at $t = 80$.

low values of C_ϕ , C_ϵ are not recommended as they would result in too much SGS energy in comparison to the resolved energy.

The computational cost of VSFDF simulations relative to those required by DNS and by the Smagorinsky model is the same as that reported previously.¹⁶ The typical ratios of

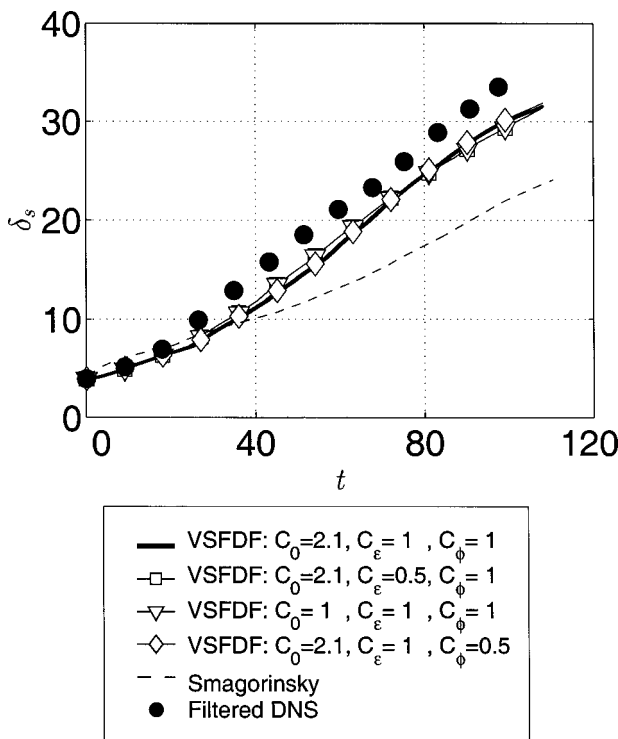


FIG. 13. Temporal variations of the scalar thickness.

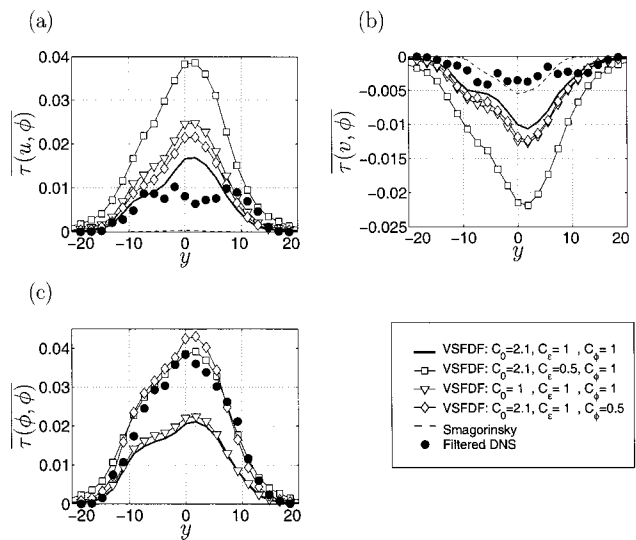


FIG. 14. Cross-stream variations of some of the components of τ at $t = 60$.

the normalized Smagorinsky–VSFDF–DNS run times are $1 - \mathcal{O}(30) - \mathcal{O}(200)$.

VI. SUMMARY AND CONCLUDING REMARKS

The filtered density function (FDF) methodology has proven effective for LES of turbulent reactive flows. In previous investigations, either the marginal FDF of the scalar, or that of the velocity were considered. The objective of present work is to develop the joint velocity-scalar FDF methodology. For this purpose, the exact transport equation governing the evolution of VSFDF is derived. It is shown that effects of the SGS convection and chemical reaction appear in a closed form. The unclosed terms are modeled in a fashion similar to those typically followed in PDF methods. The modeled VSFDF transport equation is solved numerically via a Lagrangian Monte Carlo (MC) scheme via consideration of a system of equivalent stochastic differential equations

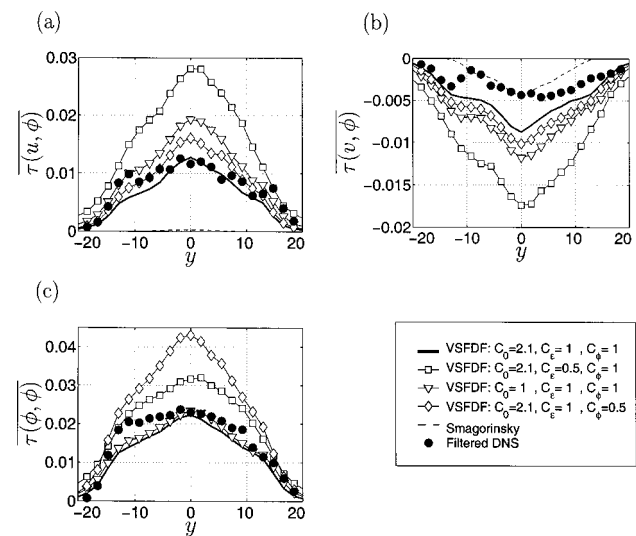


FIG. 15. Cross-stream variations of some of the components of τ at $t = 80$.

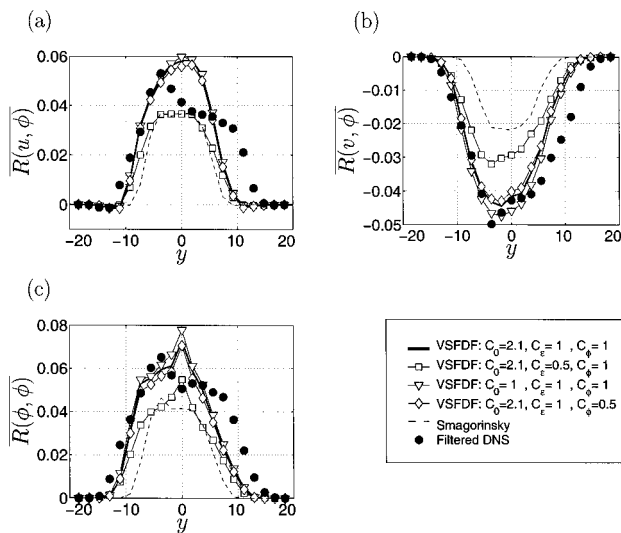


FIG. 16. Cross-stream variations of some of the components of \bar{R} at $t = 60$.

(SDEs). These SDEs are discretized via the Euler–Maruyama approximation. The consistency of the VSFDF method and the convergence of its MC solutions are assessed in LES of a two-dimensional (2D) temporally developing mixing layer. This assessment is done by comparing the results obtained by the MC procedure with those of the finite-difference scheme (LES–FD) for the solution of the transport equations of the first two moments of VSFDF. By including the third moments from the VSFDF into the LES–FD, the consistency and convergence of the MC solution are demonstrated by good agreements of the first two SGS moments with those obtained by LES–FD.

The VSFDF predictions are compared with LES results with the Smagorinsky¹⁸ SGS model. All of these results are also compared with direct numerical simulation (DNS) data of a three-dimensional, temporally developing mixing layer.

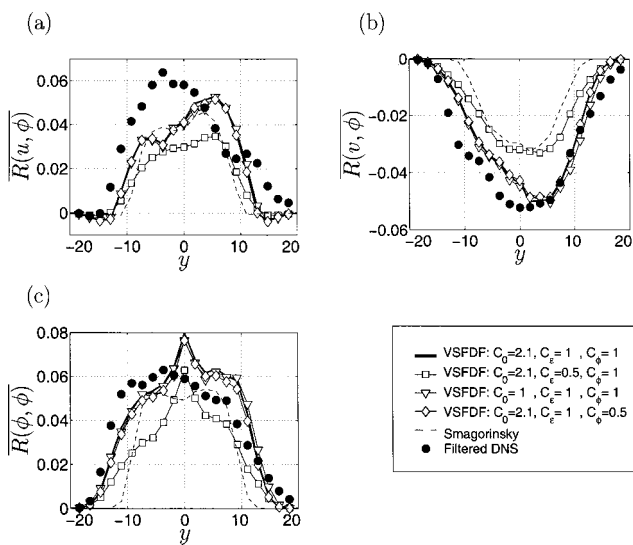


FIG. 17. Cross-stream variations of some of the components of \bar{R} at $t = 80$.

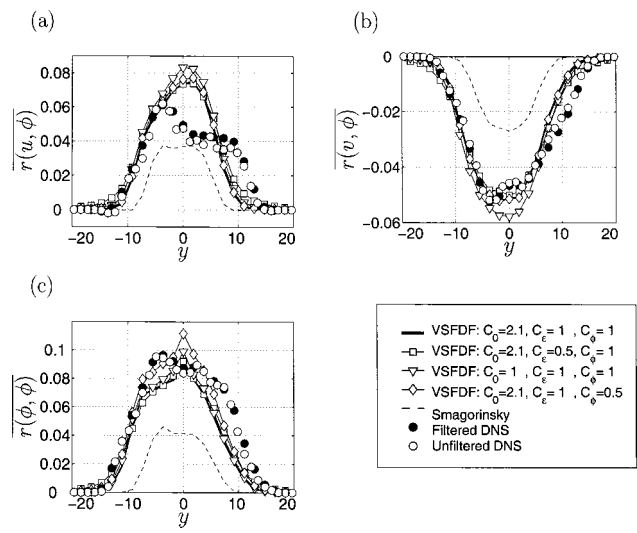


FIG. 18. Cross-stream variations of $\bar{\tau}$ at $t = 60$.

It is shown that the VSFDF performs well in predicting some of the phenomena pertaining to the SGS transport. Most of the overall flow features, including the mean field, the resolved and total stresses as predicted by VSFDF are in good agreement with DNS data. However, the model does require the input of three empirical constants. Also, the numerical implementation of VSFDF is more expensive than the traditional models. It may be possible to improve the predictive capabilities of the VSFDF by two ways: (1) development of a dynamic procedure to determine the model coefficients, and/or (2) implementation of higher order closures for the generalized Langevin model parameter G_{ij} .⁵⁰ Future work is recommended for development and application of the joint filtered velocity-scalar mass density function (VSFMDF) to allow for LES of variable density flows with/without the presence of chemical reaction.

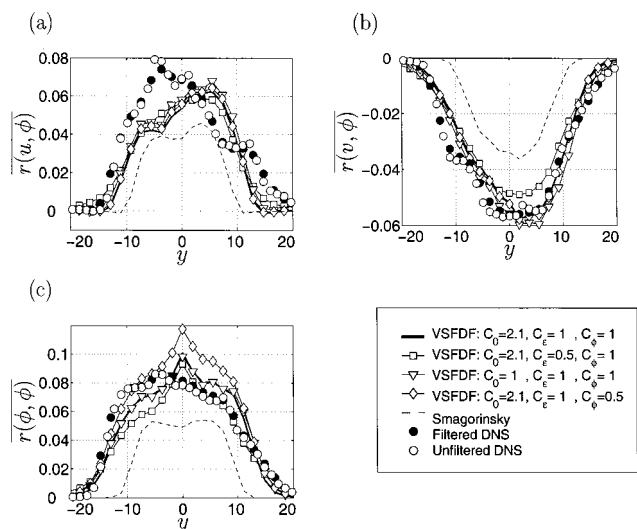


FIG. 19. Cross-stream variations of $\bar{\tau}$ at $t = 80$.

ACKNOWLEDGMENTS

The authors are indebted to Dr. P. J. Colucci, Dr. T. D. Dreeben, Dr. M. Germano, Dr. L. Y. M. Gicquel, Dr. S. Heinz, Dr. M. Lesieur, Dr. H. Steiner, and Dr. C. Tong for their excellent and very valuable comments on the first draft of this manuscript. Part of this work was conducted when the first three authors were at the State University of New York at Buffalo. The work is sponsored by the U.S. Air Force Office of Scientific Research under Grant No. F49620-03-1-0022 to University of Pittsburgh and Grant No. F49620-03-1-0015 to Cornell University. Dr. Julian M. Tishkoff is the Program Manager for both these grants. Additional support for the work at University of Pittsburgh is provided by the NASA Langley Research Center under Grant No. NAG-1-03010 with Dr. J. Philip Drummond as the Technical Monitor. Computational resources are provided by the NCSA at the University of Illinois at Urbana and by the Pittsburgh Supercomputing Center (PSC).

- ¹S. B. Pope, *Turbulent Flows* (Cambridge University Press, Cambridge, UK, 2000).
- ²S. B. Pope, "Computations of turbulent combustion: Progress and challenges," *Proc. Combust. Inst.* **23**, 591 (1990).
- ³C. K. Madnia and P. Givi, "Direct numerical simulation and large eddy simulation of reacting homogeneous turbulence," in *Large Eddy Simulations of Complex Engineering and Geophysical Flows*, edited by B. Galperin and S. A. Orszag (Cambridge University Press, Cambridge, UK, 1993), Chap. 15, pp. 315–346.
- ⁴F. Gao and E. E. O'Brien, "A large-eddy simulation scheme for turbulent reacting flows," *Phys. Fluids A* **5**, 1282 (1993).
- ⁵S. H. Frankel, V. Adumitroaie, C. K. Madnia, and P. Givi, "Large eddy simulations of turbulent reacting flows by assumed PDF methods," in *Engineering Applications of Large Eddy Simulations*, edited by S. A. Ragab and U. Piomelli (ASME, New York, 1993), FED-Vol. 162, pp. 81–101.
- ⁶A. W. Cook and J. J. Riley, "A subgrid model for equilibrium chemistry in turbulent flows," *Phys. Fluids* **6**, 2868 (1994).
- ⁷P. J. Colucci, F. A. Jaber, P. Givi, and S. B. Pope, "Filtered density function for large eddy simulation of turbulent reacting flows," *Phys. Fluids* **10**, 499 (1998).
- ⁸J. Réveillon and L. Vervisch, "Subgrid-scale turbulent micromixing: Dynamic approach," *AIAA J.* **36**, 336 (1998).
- ⁹F. A. Jaber, P. J. Colucci, S. James, P. Givi, and S. B. Pope, "Filtered mass density function for large eddy simulation of turbulent reacting flows," *J. Fluid Mech.* **401**, 85 (1999).
- ¹⁰S. C. Garrick, F. A. Jaber, and P. Givi, "Large eddy simulation of scalar transport in a turbulent jet flow," in *Recent Advances in DNS and LES, Fluid Mechanics and its Applications*, edited by D. Knight and L. Sakell (Kluwer Academic, Dordrecht, 1999), Vol. 54, pp. 155–166.
- ¹¹S. James and F. A. Jaber, "Large scale simulations of two-dimensional nonpremixed methane jet flames," *Combust. Flame* **123**, 465 (2000).
- ¹²X. Y. Zhou and J. C. F. Pereira, "Large eddy simulation (2D) of a reacting plan mixing layer using filtered density function," *Flow, Turbul. Combust.* **64**, 279 (2000).
- ¹³K. H. Luo, "DNS and LES of turbulence-combustion interactions," see Geurts (Ref. 24), Chap. 14, pp. 263–293.
- ¹⁴T. Poinsot and D. Veynante, *Theoretical and Numerical Combustion* (R. T. Edwards, Philadelphia, PA, 2001).
- ¹⁵C. Tong, "Measurements of conserved scalar filtered density function in a turbulent jet," *Phys. Fluids* **13**, 2923 (2001).
- ¹⁶L. Y. M. Gicquel, P. Givi, F. A. Jaber, and S. B. Pope, "Velocity filtered density function for large eddy simulation of turbulent flows," *Phys. Fluids* **14**, 1196 (2002).
- ¹⁷P. Givi, "A review of modern developments in large eddy simulation of turbulent reacting flows," in *DNS/LES-Progress and Challenges*, edited by C. Liu, L. Sakell, and R. Herklotz (Greyden, Columbus, OH, 2001), pp. 81–92.
- ¹⁸J. Smagorinsky, "General circulation experiments with the primitive equations. I. The basic experiment," *Mon. Weather Rev.* **91**, 99 (1963).
- ¹⁹*Turbulent Reacting Flows, Topics in Applied Physics*, edited by P. A. Libby and F. A. Williams (Springer-Verlag, Heidelberg, 1980), Vol. 44.
- ²⁰S. B. Pope, "PDF methods for turbulent reactive flows," *Prog. Energy Combust. Sci.* **11**, 119 (1985).
- ²¹R. W. Bilger, "Molecular transport effects in turbulent diffusion flames at moderate Reynolds number," *AIAA J.* **20**, 962 (1982).
- ²²U. Piomelli, "Large-eddy simulation: Achievements and challenges," *Prog. Aerosp. Sci.* **35**, 335 (1999).
- ²³C. Meneveau and J. Katz, "Scale-invariance and turbulence models for large-eddy simulations," *Annu. Rev. Fluid Mech.* **32**, 1 (2000).
- ²⁴*Modern Simulation Strategies for Turbulent Flow*, edited by B. J. Geurts (R. T. Edwards, Philadelphia, PA, 2001).
- ²⁵P. Sagaut, *Large Eddy Simulation for Incompressible Flows* (Springer, New York, 2001).
- ²⁶E. E. O'Brien, "The probability density function (PDF) approach to reacting turbulent flows," see Libby and Williams (Ref. 19), Chap. 5, pp. 185–218.
- ²⁷B. Vreman, B. Geurts, and H. Kuerten, "Realizability conditions for the turbulent stress tensor in large-eddy simulation," *J. Fluid Mech.* **278**, 351 (1994).
- ²⁸S. Karlin and H. M. Taylor, *A Second Course in Stochastic Processes* (Academic, New York, 1981).
- ²⁹N. Wax, *Selected Papers on Noise and Stochastic Processes* (Dover, New York, 1954).
- ³⁰C. W. Gardiner, *Handbook of Stochastic Methods* (Springer-Verlag, New York, 1990).
- ³¹D. C. Haworth and S. B. Pope, "A generalized Langevin model for turbulent flows," *Phys. Fluids* **29**, 387 (1986).
- ³²T. D. Dreeben and S. B. Pope, "Probability density function and Reynolds-stress modeling of near-wall turbulent flows," *Phys. Fluids* **9**, 154 (1997).
- ³³H. Risken, *The Fokker-Planck Equation, Methods of Solution and Applications* (Springer-Verlag, New York, 1989).
- ³⁴S. B. Pope, "Mean field equations in PDF particle methods for turbulent reactive flows," Technical Report FDA 97-06, Cornell University, Ithaca, NY, 1997.
- ³⁵M. Muradoglu, P. Jenny, S. B. Pope, and D. A. Caughey, "A consistent hybrid-volume/particle method for the PDF equations of turbulent reactive flows," *J. Comput. Phys.* **154**, 342 (1999).
- ³⁶M. Muradoglu, S. B. Pope, and D. A. Caughey, "The hybrid method for the PDF equations of turbulent reactive flows: Consistency conditions and correction algorithms," *J. Comput. Phys.* **172**, 841 (2001).
- ³⁷P. E. Kloeden, E. Platen, and H. Schurz, *Numerical Solution of Stochastic Differential Equations Through Computer Experiments* (Springer-Verlag, New York, 1997).
- ³⁸I. I. Gikhman and A. V. Skorokhod, *Stochastic Differential Equations* (Springer-Verlag, New York, 1972).
- ³⁹M. H. Carpenter, "A high-order compact numerical algorithm for supersonic flows," in *Twelfth International Conference on Numerical Methods in Fluid Dynamics, Lecture Notes in Physics*, edited by K. W. Morton (Springer-Verlag, New York, 1990), Vol. 371, pp. 254–258.
- ⁴⁰C. A. Kennedy and M. H. Carpenter, "Several new numerical methods for compressible shear-layer simulations," *Appl. Numer. Math.* **14**, 397 (1994).
- ⁴¹J. J. Riley and R. W. Metcalfe, "Direct numerical simulations of a perturbed, turbulent mixing layer," *AIAA Paper* 80-0274 (1980).
- ⁴²N. D. Sandham and W. C. Reynolds, "Three-dimensional simulations of large eddies in the compressible mixing layer," *J. Fluid Mech.* **224**, 133 (1991).
- ⁴³R. D. Moser and M. M. Rogers, "The three-dimensional evolution of a plane mixing layer: Pairing and transition to turbulence," *J. Fluid Mech.* **247**, 275 (1993).
- ⁴⁴B. Vreman, B. Geurts, and H. Kuerten, "Large-eddy simulation of the turbulent mixing layer," *J. Fluid Mech.* **339**, 357 (1997).
- ⁴⁵R. W. Metcalfe, S. A. Orszag, M. E. Brachet, S. Menon, and J. J. Riley, "Secondary instabilities of a temporally growing mixing layer," *J. Fluid Mech.* **184**, 207 (1987).
- ⁴⁶S. J. Lin and G. M. Corcos, "The mixing layer: Deterministic models of a turbulent flow. Part 3. The effect of plane strain on the dynamics of streamwise vortices," *J. Fluid Mech.* **141**, 139 (1984).
- ⁴⁷R. D. Moser and M. M. Rogers, "The three-dimensional evolution of a plane mixing layer: the Kelvin-Helmholtz rollup," *J. Fluid Mech.* **243**, 183 (1992).

- ⁴⁸R. D. Moser and M. M. Rogers, "Spanwise scale selection in plane mixing layers," *J. Fluid Mech.* **247**, 321 (1993).
- ⁴⁹G. Erlebacher, M. Y. Hussaini, C. G. Speziale, and T. A. Zang, "Toward the large eddy simulation of compressible turbulent flows," *J. Fluid Mech.* **238**, 155 (1992).
- ⁵⁰S. B. Pope, "On the relation between stochastic Lagrangian models of turbulence and second-moment closures," *Phys. Fluids* **6**, 973 (1994).
- ⁵¹R. S. Rogallo and P. Moin, "Numerical simulation of turbulent flow," *Annu. Rev. Fluid Mech.* **16**, 99 (1984).
- ⁵²R. W. Bilger, "Future progress in turbulent combustion research," *Prog. Energy Combust. Sci.* **26**, 367 (2000).
- ⁵³N. Peters, *Turbulent Combustion* (Cambridge University Press, Cambridge, UK, 2000).